Geochemical Journal, Vol. 47, pp. 285 to 307, 2013

Mineralogy, fluid inclusion and stable isotope constraints on the genesis of the Namseong Au–Ag deposit, Republic of Korea

BONG CHUL YOO[1] and NOEL C. WHITE[2]*

[1]Mineral Resources Research Department, Mineral Resources Research Division, Korea Institute of Geoscience and Mineral Resources, Daejon 305-350, Republic of Korea
[2]CODES, University of Tasmania, Hobart Tas 7000, Australia

(*Received March 21, 2012; Accepted January 1, 2013*)

The Namseong gold and silver deposit is located in the Seolcheon metallogenic province, one of the most important gold production areas in the Republic of Korea. It consists of three gold and silver-bearing quartz veins that fill fractures oriented NW along fault zones in Triassic porphyritic granite. The gold and silver-bearing quartz veins are simple and consist of only one mineralization stage on basis of vein mineralogy and paragenesis. Coarse-grained quartz is found in mainly comb, and partially cockade and cavity-filling textures throughout most of the veins. Wall-rock alteration minerals include sericite, minor pyrite and chlorite. Ore minerals deposited along with electrum include pyrite, sphalerite, chalcopyrite, galena, pyrargyrite, argentite and native silver. Its mineralization age (78.2 ± 1.7 Ma) determined on sericite from wall-rock alteration indicates that the gold and silver mineralization was synchronous with Cretaceous igneous activity.

Petrographic examination of textural relationships among sulfides, fluid inclusions, and quartz from one stage shows the genetic relationships between Au–Ag deposition and fluid entrapment. Early wall-rock alteration in one stage was produced and sulfides were deposited from H_2O–NaCl–CO_2 fluids (260–1,700 bar, average 1,000 bar) with Th_{total} values of 250°C to 380°C and salinities less than about 4 wt.% NaCl. The late sulfides and electrum in one stage were deposited from H_2O–NaCl fluids (100 bar) with Th_{total} values of 195°C to 331°C and salinities less than about 7 wt.% NaCl. The H_2O–NaCl fluids either evolved through unmixing of H_2O–NaCl–CO_2 fluids or through mixing with circulating meteoric waters as a result of uplift or unloading during mineralization, or both. The deposition of electrum and silver minerals was caused by a decrease in sulfur fugacity/aH_2S/aCl, oxygen fugacity and temperature during wallrock alteration, cooling and dilution produced by mixing of the saline aqueous fluids with meteoric water.

The calculated sulfur isotope compositions of hydrothermal fluids from the Namseong deposit ($\delta^{34}S_{H2S}$ = 3.7‰ to 7.2‰) indicate that ore sulfur was derived mainly from a magmatic source but also in part from sulfur contained in the host rocks. The calculated and measured oxygen and hydrogen isotope compositions of the ore-forming fluids ($\delta^{18}O_{H2O}$ = –2.2‰ to 1.6‰, δD = –83‰ to –64‰) indicate that the fluids were derived from meteoric water and evolved by mixing with local meteoric water and by limited water-rock exchange during mineralization in uplift zones.

Keywords: Cretaceous quartz vein, mineralogy, fluid inclusions, stable isotopes, mixing

INTRODUCTION

The Namseong Au–Ag deposit is located in the Seolcheon metallogenic province, one of ten metallogenic provinces in the Republic of Korea recognized by Kim (1970) (Fig. 1a). This metallogenic province that contains more than sixty Au–Ag deposits has been one of the most important gold producers in the Republic of Korea. Eighteen Au–Ag deposits are located near the Namseong deposit. Inferred ore resources from the eighteen deposits are estimated at about 1.1 million tonnes of ore and the deposits are associated temporally and spatially with Jurassic and Cretaceous igneous activity (Kim, 1970; Choi *et al*., 2005, 2006).

The many gold-silver deposits in the Seolcheon metallogenic province can be divided into mainly Jurassic gold deposits (Samdong and Samhwanghak) and Cretaceous gold-silver deposits (Yonghwa, Weolseong, Soowang and Weolyu) (Youn and Park, 1991, 1993, 2004; Yun *et al*., 1993; Lee *et al*., 1994; So *et al*., 1995; So and Yun, 1997). The Jurassic gold deposits were formed at intermediate crustal depths, probably between 8 and 12 km, related spatially and temporally to deep-seated granitoids, whereas the Cretaceous gold-silver deposits were formed within a few kilometres of the surface re-

*Corresponding author (e-mail: noelcwhite@hotmail.com)

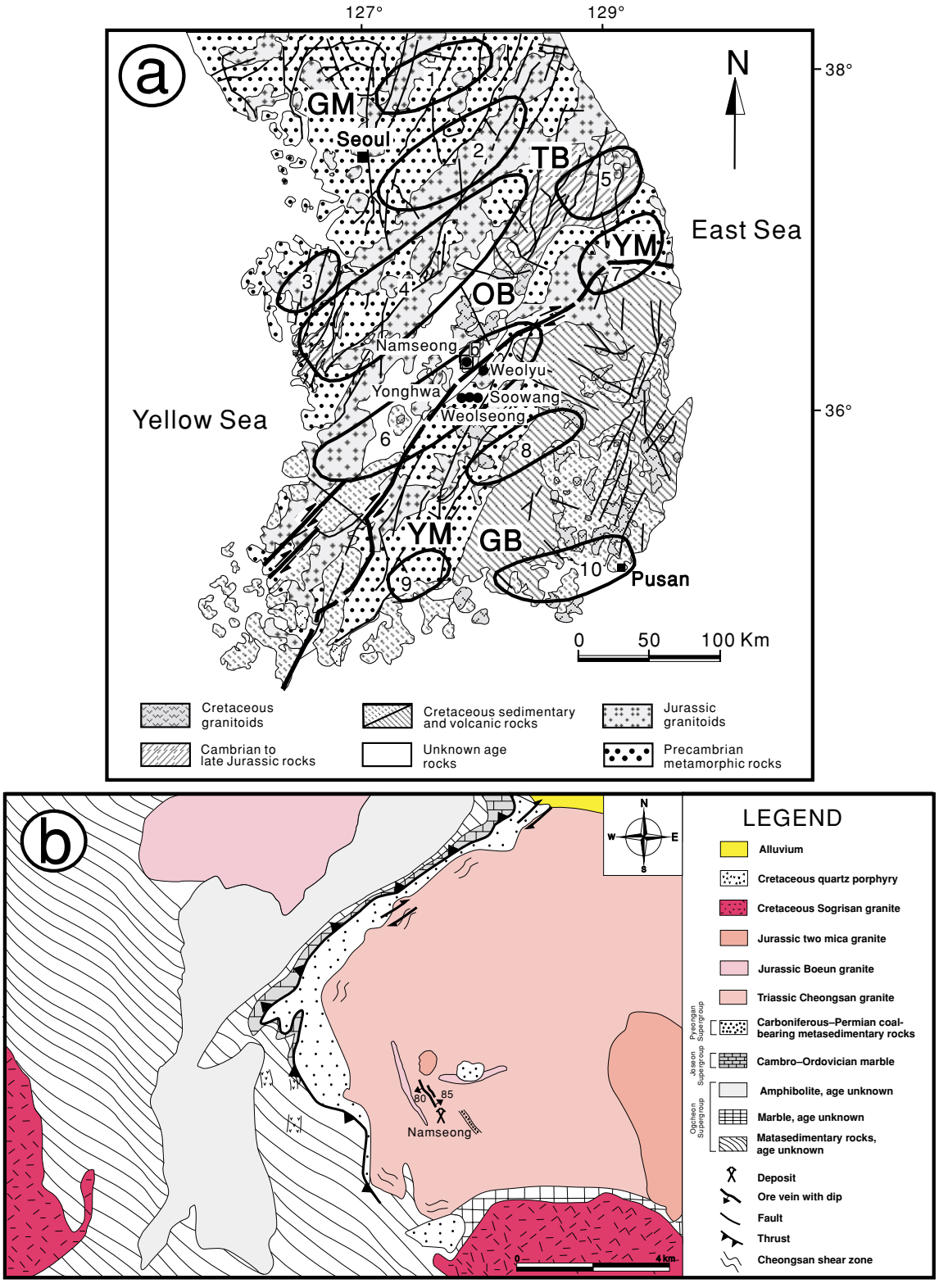

Fig. 1. a) Simplified geological map of the Republic of Korea, showing the distribution of ten gold-silver metallogenic provinces (1, Pocheon; 2, Hongcheon; 3, Haemi; 4, Cheonan; 5, Jeongseon; 6, Seolcheon; 7, Bonghwa; 8, Hapcheon; 9, Suncheon-Gwangyang; 10, Haman-Gunbuk), Jurassic and Cretaceous granitoids, and major faults. GM, Gyeonggi massif; YM, Yeongnam massif; OB, Ogcheon belt; TB, Taebaeg belt; GB, Gyeongsang basin. Solid circles indicate gold-silver deposits. Black lines indicate faults. Bold black lines indicate Honam shear zone. Solid squares indicate city (modified from Kim (1970) and Choi et al. (2005)). b) Generalized geological map of the Namseong deposit, showing the orientation of the principal quartz vein.

lated spatially and temporally to shallow-level Cretaceous granitoids (110–145 Ma; Choi *et al*., 2005). The gold-silver deposits commonly have complex vein morphologies, complex mineralogy, and high silver/gold ratios (Choi *et al*., 2001). These deposits formed in strike-slip faults and caldera-related fractures related to subvolcanic activity that was associated spatially and temporally with reactivation of major strike-slip faults by oblique to orthogonal convergence in a continental arc setting (Choi *et al*., 2006).

The Namseong deposit operated intermittently from 1927 to 1965 and produced 21,823 g of gold and 156,387 g of silver from 437 t of ore from 1962 to 1965. The deposit was again worked from 1980 to 1985 by underground workings over a length of 700 m and to a vertical depth of up to 70 m. The deposit produced 200 t of ore per year. It was again operated intermittently on five levels and produced 141,123 t of ore from 1997 to 2005 yielding 570 g of gold and 7,520 g of silver in 2002. The ore had an average grade of about 4–5 g/t Au and 120–125 g/t Ag.

Previous investigations at the Namseong deposit by KMPC (Korea Mining Promotion Corporation) (1973, 1983, 1987), Lee *et al*. (1987) and Choi *et al*. (1988) focused on the general geology and ore mineralogy. This study is based mainly on samples collected from underground and thus present an opportunity to investigate mineralogy, fluid inclusions, and stable isotope compositions of the gold- and silver-bearing quartz veins to ascertain the conditions of mineralization and the potential sources of the vein-forming fluids, and to compare the characteristics of the Namseong deposit with those of Cretaceous gold-silver deposits (Yonghwa, Weolseong, Soowang and Weolyu) elsewhere in the Seolcheon metallogenic province.

Geologic Setting

The geological architecture of the Republic of Korea consists dominantly of the Precambrian Gyeonggi massif (GM), the Paleozoic Ogcheon belt (OB), the Paleozoic Taebaeg belt (TB), the Precambrian Yeongnam massif (YM), Jurassic granitoids, the Cretaceous Gyeongsang basin (GB), and Cretaceous granitoids (Fig. 1a). The Gyeonggi and Yeongnam massifs are composed of gneiss and schist. The Ogcheon belt consists of low- to medium-grade metasedimentary and metavolcanic rocks. The Taebaeg belt consists of non- to weakly metamorphosed sedimentary rocks. The Jurassic granitoids are distributed along NE- or NNE-trending batholithic belts and are characterized by meso- or katazone emplacement and no major volcanic activity. The Jurassic granitoids are metaluminous to peraluminous in composition and belong to the calc–alkaline and ilmenite–magnetite series, and generally show I-type characteristics (Sagong *et al*., 2005). The Gyeongsang basin consists of sedimentary and calc–alkaline volcanic rocks deposited in a continental arc setting (Chough *et al*., 2000). The Cretaceous granitoids occur mostly in the Gyeongsang basin, and partially in the central part of the Ogcheon and Taebaeg belts. They typically display miarolitic cavities, and porphyritic and micrographic textures indicating shallow intrusive origins (<11 km; Oh, 2006) and are interpreted to be co-magmatic with the Yucheon volcanic rocks (Lee *et al*., 1987). They are metaluminous to peraluminous in composition and belong to the calc–alkaline and magnetite series, and generally show I-type characteristics (Jwa, 1996). This magmatic activity was triggered by northwest-directed subduction of the Izanagi plate (Choi *et al*., 2005).

The oldest rocks at the Namseong deposit are metasedimentary rocks of the Ogcheon Supergroup (Fig. 1b). They are distributed along a NNW trend west of the deposit and consist of mainly phyllite and partly slate that exhibit gradational contacts. They strike N20–45°W and dip 30–60°SW and are composed of quartz, feldspar, biotite and chlorite. Marble of the Ogcheon Supergroup is distributed along an E–W trend south of the deposit. Amphibolite of the Ogcheon Supergroup is distributed along a NNW trend west of the deposit and shows relic igneous textures. It is interpreted to have been emplaced in an intraplate rift environment based on geochemical data (Kwon and Lee, 1992). Marble of the Joseon Supergroup is distributed along a NNW trend west of the deposit. Meta-psammites of the Pyeongan Supergroup are distributed along a NNW trend west of the deposit and occur as a small roof pendant NE of the deposit. They were intruded by Triassic porphyritic granite (Cheongsan granite). The meta-psammite mainly comprises quartzite and is intercalated with dark grey coal-bearing shale, and is composed of quartz, feldspar and biotite.

The granitoids in the deposit area are divided into Triassic Cheongsan granite (217 Ma using U–Pb on sphene and Rb–Sr on granite near veins), Jurassic granitoids (Boeun granite, 171 Ma using U–Pb on sphene and Rb–Sr on granite near veins; two mica granite), Jurassic two mica granite and Cretaceous Sogrisan granite (91 Ma using Rb–Sr on granite near veins; 72 Ma using K–Ar on biotite) (Yun and Kim, 1990; Jwa *et al*., 1995; Cheong and Chang, 1997; Ree *et al*., 2001). The Cheongsan granite occupies most of the deposit area and intruded metasedimentary rocks of the Ogcheon, Jocheon and Pyeongan Supergroups (Fig. 1b). It is coarse to medium grained with porphyritic, poikilitic and myrmekitic textures and is characterized by K-feldspar megacrysts of orthoclase or microcline. The volume of megacrysts ranges from 17% to 42% with an average of 28% (Sagong and Jwa, 1997). The lengths of the megacrysts are 2–8

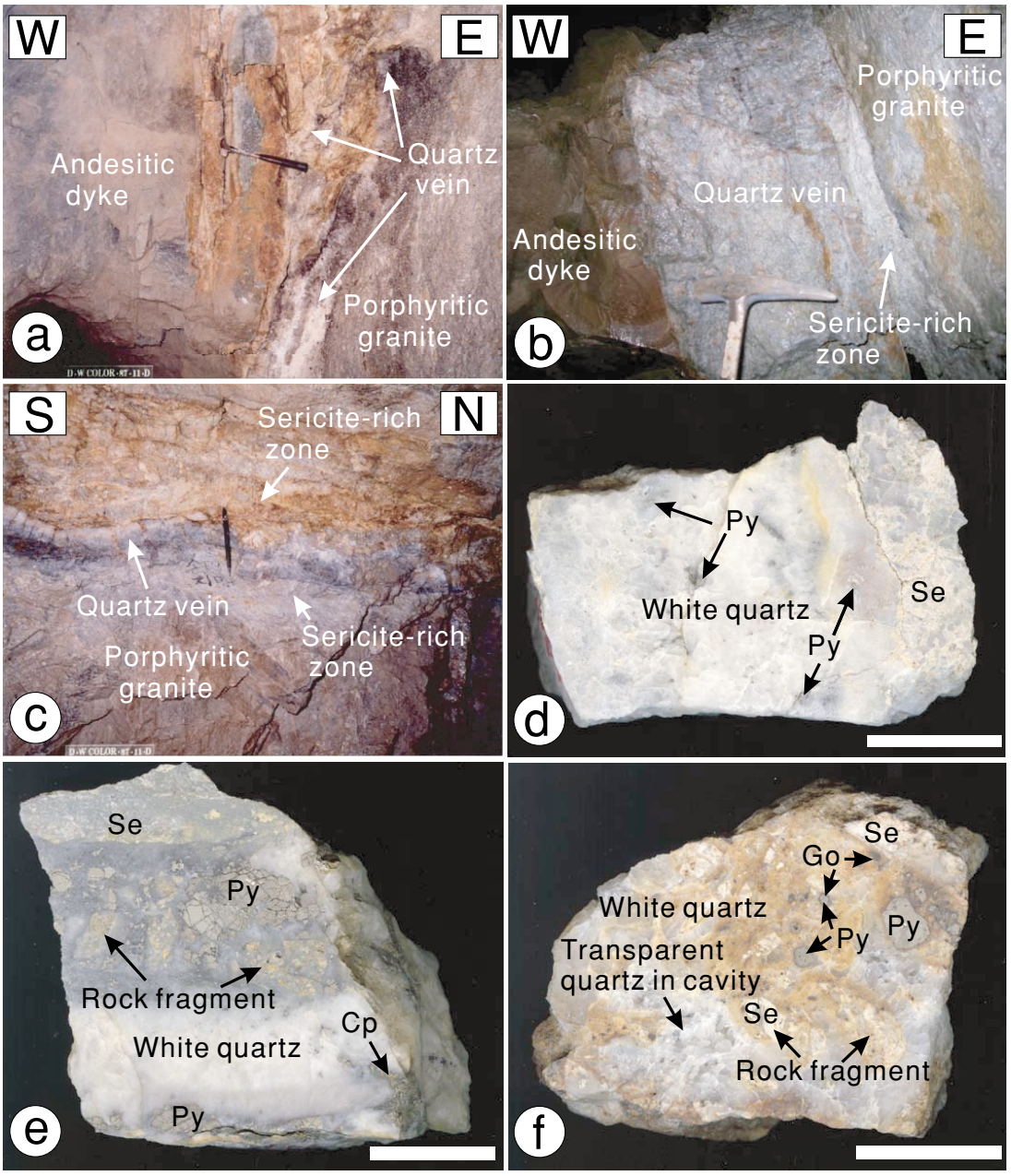

Fig. 2. Photographs of mineralized quartz veins and alteration of wall-rock exposed underground in the Namseong deposit. a) Quartz vein and sericite alteration of wall-rock. b) Close-up of quartz vein and sericite alteration. c) Quartz vein shows comb texture, and fragments of wall-rock are altered to sericite and quartz. d) and e) Wall-rock alteration and ore minerals in white quartz. f) Wall-rock fragment cockade and cavity textures and ore minerals in white and transparent quartz. Cp, chalcopyrite; Go, goethite; Py, pyrite; Se, sericite. Scale bar is 4 cm in length.

cm with a maximum of up to 15 cm. The matrix consists of K-feldspar (4.4–36.0%), plagioclase (5.9–25.2%), quartz (17.9–44.6%), and biotite (4.1–19.3%) with minor amounts of allanite, zircon, rutile, apatite and titanate. Plagioclase grains are euhedral to subhedral and are oligoclase to andesine in composition (Sagong and Jwa, 1997; Ree *et al*., 2001; Kwon *et al*., 2009). The granitoid is metaluminous and belongs to the calc–alkaline and ilmenite series, and generally is I-type granite that was originated in a continental margin setting (Sagong and Jwa, 1997).

The Jurassic Boeun granite intruded metasedimentary rocks of the Ogcheon Supergroup and is distributed along a NNW trend northwest of the deposit (Fig. 1b). It is

medium grained and consists of plagioclase, quartz, K-feldspar, and biotite with minor amounts of sphene, apatite, zircon, allanite and ilmenite (Cho *et al*., 1994). It is metaluminous and belongs to the calc–alkaline series, and generally is I-type granite that was originated in a continental margin setting (Jwa, 1996).

The Jurassic two mica granite intruded the Cheongsan granite and is distributed southeast of the deposit (Fig. 1b). It is fine to medium grained and consists of quartz, K-feldspar, plagioclase, biotite, muscovite, apatite and zircon (Sagong and Jwa, 1997). It is peraluminous and calc–alkaline and geochemically shows both I- and S-type characteristics; it is interpreted to have originated in a continental margin setting (Sagong and Jwa, 1997). The Sogrisan granite, which is divided into coarse grained biotite granite, porphyritic granite and granite porphyry, intruded metasedimentary rocks of the Ogcheon Supergroup. It is distributed south of the deposit and consists of orthoclase, plagioclase, quartz and biotite (Cho *et al*., 1994; Fig. 1b). Quartz porphyry intrudes the Cheongsan granite and two mica granite, and cuts the quartz veins in the underground deposit. It strikes 20–30° and dips 80°NE, and consists of quartz, feldspar and biotite. Andesitic dike intrudes metasedimentary rocks of the Ogcheon Supergroup and the Cheongsan granite, and cuts the quartz veins in the underground deposit. It strikes 30–40° and dips 85°SW.

The main structural features in the Namseong deposit area are two NE-trending ductile shear zones (Cheongsan shear zone and Honam shear zone), a NW-dipping thrust and NW-trending fault (Figs. 1a and b). The Cheongsan shear zone is developed along the northwestern boundary of the Cheongsan granite and is observed to have subhorizontal lineations (protomylonite–ultramylonite), interpreted as an evidence for a strike-slip dominant shear zone (Ree *et al*., 2001). Ree *et al*. (2001) suggested that the Cheongsan shear zone was developed during the late stage of the middle Triassic Songrim orogeny and was formed before the Honam shear zone. Subsequently the thrust was developed parallel to the Cheonsan shear zone along the northwestern boundary of the Cheongsan granite. It was formed after emplacement of the Cheongsan granite and before emplacement of the Boeun granite (Ree *et al*., 2001). The Honam shear zone is developed along the southeastern part of the deposit, and dextral ductile shear movement of this zone took place during the Middle Jurassic Daebo orogeny (Ree *et al*., 2001). Finally, northeast of the deposit a NW-trending fault cuts across all rocks in the deposit area (Fig. 1b). It is interpreted that the fault was formed after deposition of the Cretaceous sedimentary rocks. Quartz veins in the deposit area were generated by Jurassic NW–SE regional compression and by early Cretaceous NW–SE or N–S regional compression (Sagong *et al*., 2005).

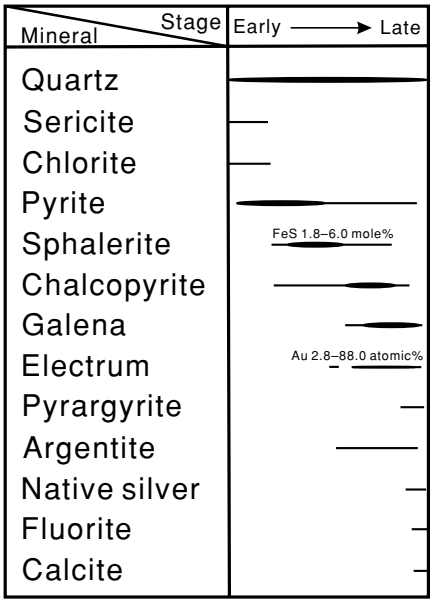

Fig. 3. Paragenetic sequence of ore, gangue and alteration minerals in veins of the Namseong deposit.

Vein Mineralization

The Namseong deposit consists of three fault-hosted gold and silver-bearing quartz veins that vary in thickness from 0.01 to 0.3 m and contain up to 4–5 g/t gold and 120–125 g/t silver. They have a general 50–60° strike and 70–85° SW/NE dip and extend strike for about 900 m, and extend to a vertical depth of more than 70 m. The gold and silver-bearing quartz veins at the Namseong deposit consist of only one stage based on field evidences and display a variety of typical open-space filling vein textures (Figs. 2a–c). Coarse-grained quartz from one stage is found in mainly comb, and partially cockade and cavity-filling textures throughout most of the veins. The quartz veins are white to transparent and commonly massive and accompany coarse pyrite bands near their margins. Based on quartz vein textures and mineralogical, textural, and crosscutting relationships of all minerals by microscopy, it is subdivided into early and late stage (Figs. 2, 3 and 4). Country rock fragments are rarely included in the veins and are strongly altered by phyllic and silicic alteration (Figs. 2b and c).

Early hydrothermal alteration around the quartz veins of only one stage consists mainly of intense sericitic, silicic, pyritic, and chloritic alteration that can extend up to 1 m from the vein margin. All the primary minerals (orthoclase, microcline, plagioclase and biotite) of the wall-rock are affected by the alteration and small pyrite crystals are scattered throughout the altered rock. Sericitic alteration is regional in extent, and adjacent to the de-

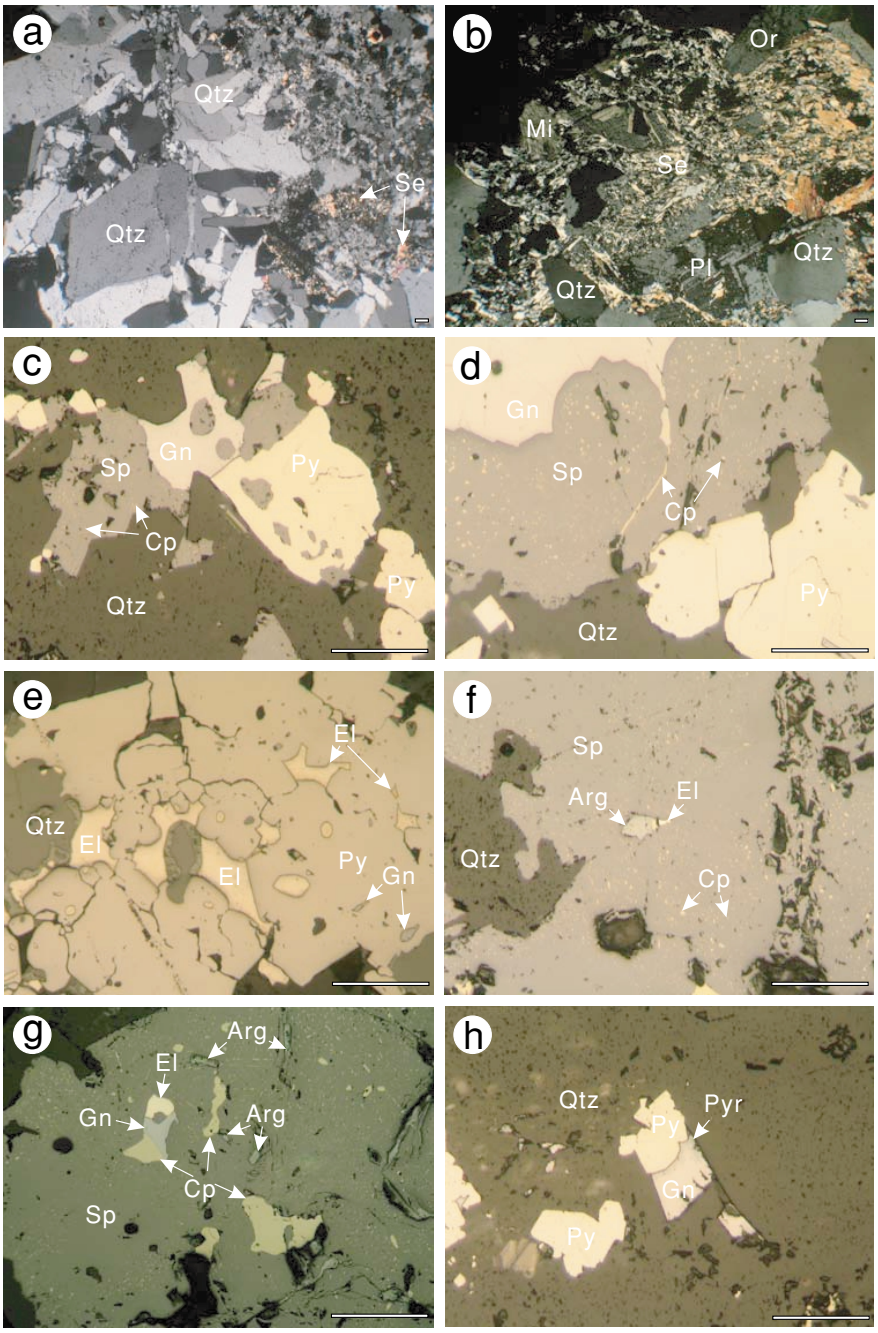

Fig. 4. Microphotographs of ore, gangue and alteration minerals representative of veins of the Namseong deposit. a) and b) Sericitic and silicic alteration at quartz vein margin. c) Pyrite and chalcopyrite-diseased sphalerite partly replaced by galena. d) Chalcopyrite and galena with sealed fractures in pyrite and chalcopyrite-diseased sphalerite. e) Electrum and galena with sealed fractures in pyrite. f) Electrum and argentite intergrown with chalcopyrite-diseased sphalerite. g) Electrum, argentite, chalcopyrite and galena with sealed fractures in chalcopyrite-diseased sphalerite. h) Galena and pyrargyrite intergrown with pyrite. Arg, argentite; Cp, chalcopyrite; El, electrum; Gn, galena; Mi, microcline; Or, orthoclase; Pl, plagioclase; Py, pyrite; Pyr, pyrargyrite; Qtz, quartz; Se, sericite; Sp, sphalerite. Scale bar is 200 μm in length.

posit grades into chloritic alteration over a distance of several centimetres. Sericitic alteration occurs along the vein margins and is characterized by replacement of microcline phenocrysts, and pervasive silicification of the groundmass. Primary textures in this alteration generally are destroyed but locally are well preserved. The sericitic alteration assemblage consists of fine-grained sericite, quartz, pyrite and calcite. Chloritic alteration replacing the original minerals consists of an assemblage of chlorite, pyrite, quartz and calcite, and generally destroys primary textures.

In order to date the mineralization using K–Ar techniques, sericite from the wall-rock alteration was extracted by elutriation in distilled water and identified by XRD. Potassium was analysed by flame photometry using a 2,000 ppm Cs buffer (Nagao *et al*., 1984). Argon was analysed on a 15 cm radius sector type mass spectrometer with a single collector system at Okayama University of Science, designed and constructed by Nagao and Itaya (1988), using an isotopic dilution method and an ^{38}Ar spike (Yin *et al*., 2002). The calculations of ages and errors for gold and silver mineralization were carried out using the method of Nagao *et al*. (1984) and Itaya *et al*. (1991). The absolute timing of gold mineralization in the Namseong deposit was 78.2 ± 1.7 Ma.

Ore Mineralogy

The ore mineralogy at the Namseong deposit has been reported by Lee *et al*. (1987). The mineralogy of the veins is simple and no spatial variability in the mineralogy of the veins was observed. The veins hosting gold and silver mineralization in the Namseong deposit consist mainly of white massive and euhedral transparent quartz (Figs. 2d–f). The paragenesis of the veins has been ascertained on the basis of mineralogical, textural, and crosscutting relationships as observed in both hand specimens and polished thin sections. In addition we undertook detailed alteration studies by petrography and XRD analyses.

Only one stage of vein fill was recognized in the Namseong deposit and its mineralogy is simple, and it is subdivided into early and late stage, illustrated schematically in Fig. 3. Wall-rock alteration minerals, pyrite and sphalerite with minor amounts of chalcopyrite were the early minerals deposited in the wall-rock alteration zone or vein margins, and lastly deposited chalcopyrite, galena with minor amounts of pyrite, sphalerite, electrum, argentite, pyrargyrite, and native silver (Figs. 2, 3 and 4). Wall-rock alteration minerals include sericite and minor pyrite, chlorite and carbonates (Figs. 4a and b). The chemical compositions of sulfides and electrum were analysed by electron microprobe spectrometry (operating voltage = 20 kV, beam current = 20 nA, counting time = 20 sec.). Calibrations were done using international standards, and data corrected using ZAF corrections.

Pyrite, the most abundant sulfide, occurs disseminated as coarse to fine grains in early altered wall-rock or as euhedral to anhedral masses alone or closely intergrown with sphalerite, chalcopyrite and electrum near vein margins. It also occurs as euhedral masses alone or closely intergrown with sphalerite, chalcopyrite, galena and electrum in vein centers. It is replaced locally by goethite. Sphalerite occurs disseminated or as fine grains closely intergrown with pyrite, chalcopyrite and electrum near the vein margins. It also occurs as disseminated, coarse or fine grains intergrown with pyrite, chalcopyrite, galena, electrum and argentite parallel to the vein centers. It also fills microfractures in early pyrite and coexists with chalcopyrite, galena and electrum. The FeS contents of sphalerite range from 1.8 to 6.0 mole% with an average of 3.6 ± 1.7 (1σ; n = 6).

Chalcopyrite occurs disseminated or as fine grains closely intergrown with pyrite, sphalerite, galena and electrum. It also fills microfractures in early pyrite. Galena is intimately intergrown with pyrite, sphalerite, chalcopyrite, and electrum, and also fills microfractures in early pyrite.

Electrum occurs as inclusions in early pyrite and is commonly intimately intergrown with late pyrite, sphalerite, chalcopyrite and galena, but it also occurs alone in quartz grains. It is also present as irregular and/or subrounded grains, commonly associated with pyrite, sphalerite, chalcopyrite, galena and quartz. In the Namseong deposit, 46.4% of electrum is associated with pyrite, 15.9% is associated with sphalerite and chalcopyrite, 22.1% is associated with galena, and 15.6% occurs free in quartz. Electrum grains range from <30 μm to >177 μm in their largest dimension. The grains contain 2.8 to 88.0 at.% Au with an average of 33.1 ± 24.4 (1σ; n = 171). Au contents of electrum grains associated with pyrite and quartz are higher than those of electrum associated with chalcopyrite and galena, suggesting that the Au content of electrum decreases through the paragenetic sequence. Argentite from the Namseong deposit is commonly intergrown intimately with sphalerite, galena, electrum and pyrargyrite. Rare pyrargyrite and native silver from the Namseong deposit are commonly intergrown with chalcopyrite, galena and electrum.

Fluid Inclusion Studies

White and transparent samples of quartz from the veins at the Namseong deposit were prepared as 100 μm thick doubly polished sections for fluid inclusion study. Twenty-one double-polished sections were examined petrographically and of these, sixteen were selected for microthermometric analysis. Microthermometric analyses were performed on a Linkam THMSG 600 system

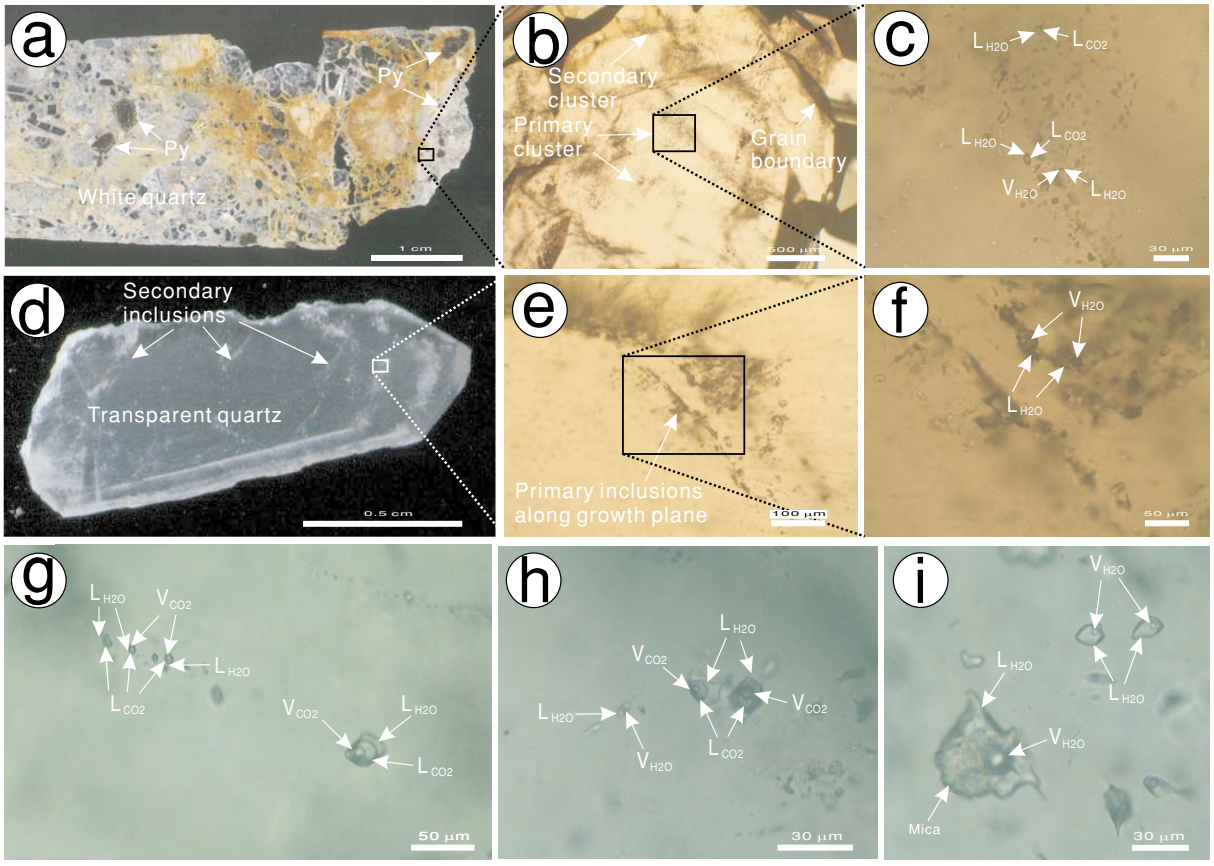

Fig. 5. Photomicrographs of representative fluid inclusion types in quartz from the Namseong deposit. a) to c) Primary cluster of types I and II inclusions showing random orientation within single quartz grains in white quartz related to wall-rock alteration. d) to f) Primary type II inclusions along growth zones in transparent quartz. g) and h) Type Ia (liquid H_2O + liquid CO_2), type Ib (liquid H_2O + liquid CO_2 + vapor CO_2) and type IIa (liquid H_2O-rich + vapor H_2O) inclusions in white quartz; (i) Type IIa (liquid H_2O-rich + vapor H_2O) and type IIb (liquid H_2O-rich + vapor H_2O-mica) inclusions in transparent quartz.

attached to a Nikon transmitted-light microscope. During freezing experiments a sequential freezing technique was employed (Haynes, 1985). Heating rates were maintained near 2°C/min for measurements of homogenization temperatures (Th_{total}). Precision is calculated as ±0.1°C in the temperature range of the observed phase changes. Accuracy between –80°C and –10°C is estimated to be ±0.2°C, whereas between –10°C and +30°C and above +100°C, is ±0.5°C and ±2°C, respectively. Instrumental calibration was done using synthetic pure H_2O and pure CO_2 inclusion standards.

Petrography, Distribution, and Types

Petrographic studies and analyses of fluid inclusions were carried out based on fluid inclusion assemblages (Goldstein and Reynolds, 1994; Goldstein, 2001) and fluid inclusion petrography, following the methodologies of Van den Kerkhof and Hein (2001) and Bodnar (2003). If the fluid inclusions were trapped along mineral growth planes in quartz, or along the same healed cracks, we concluded that these inclusions were trapped synchronously and therefore represent a true fluid inclusion assemblage, and were classified as primary, pseudosecondary or secondary using the usual criteria (Roedder, 1984; Goldstein and Reynolds, 1994). The relative timing and trapping history of the fluid inclusions were also estimated using the usual criteria (Roedder, 1984; Shepherd *et al.*, 1985; Goldstein and Reynolds, 1994; Goldstein, 2001; Bodnar, 2003). Fluid inclusions were found in white and transparent vein quartz, and isolated or as scattered groups or clusters containing similar liquid/vapor ratios in single grains, mineral growth planes or the same healed cracks. Where clusters of fluid inclusions showed similar heating and freezing behaviour, we infer that these inclusions were trapped synchronously from the same fluids.

Fluid inclusions from the Namseong deposit consist of two compositional types, aqueous and aqueous–

Table 1. Summary of microthermometric data for measured fluid inclusions from the Namseong deposit

Inclusion type	Type Ia (2 phase)	Type Ib (3 phase)	Type IIa (2 phase)	Type IIb (3 phase)
Composition	H_2O–CO_2–CH_4, low salinity	H_2O–CO_2–CH_4, low salinity	H_2O–NaCl, low salinity	H_2O–NaCl, low salinity
V_{VAP} (%)	40 to 90	40 to 90	5 to 30	10 to 30
Tm_{CO2} (°C)	–57.9 to –56.6 (–57.0 ± 0.4)	–57.5 to –56.6 (–56.7 ± 0.2)		
$Tm_{clathrate}$ (°C)	8.6 to 10.8 (9.3 ± 0.6)	7.8 to 10.1 (8.5 ± 0.6)		
Tm_{ice} (°C)			–4.4 to 0.0 (–1.3 ± 1.1)	–3.4 to –0.2 (–1.6 ± 1.0)
Th_{CO2}(L) (°C)	17.3 to 24.6 (21.7 ± 2.2)	25.2 to 30.9 (28.5 ± 1.7)		
Th_{total} (°C)	286 to 345 (312 ± 21)	250 to 380 (316 ± 29)	104 to 342 (244 ± 43)	120 to 260 (213 ± 43)
Th_{total}(L) (°C)	286 to 345 (307 ± 24)	257 to 354 (321 ± 38)	104 to 342 (244 ± 43)	120 to 260 (213 ± 43)
Th_{total}(V) (°C)	289 to 336 (317 ± 17)	250 to 380 (314 ± 26)		

carbonic inclusions (Figs. 5a–i), with the former more abundant than the latter (Figs. 5a–c, g and h). Various types of inclusions were distinguished on the basis of their appearance at room temperature (25°C), combined with their cooling behaviour down to about –50°C and their low temperature response on heating to about 32°C.

Type I are aqueous–carbonic inclusions that occur as isolated inclusions or as clusters within single quartz grains, together with aqueous inclusions. These fluid inclusions are only observed in early white quartz from the sericite-rich zone of the vein margins. Their diameters are less than 40 μm and most range from 10 to 30 μm. At 25°C they consist of two phases (liquid water + liquid CO_2 = type Ia) or in some cases three (liquid water + liquid CO_2 + vapor CO_2 = type Ib; Figs. 5a–c, g and h). Type I inclusions occur as negative crystals or as subrounded or elongate shapes, indicating a primary and/or pseudosecondary origin. Their CO_2 volumetric proportion ranges from 60 to 90 percent, with most having from 70 to 80 volume percent CO_2.

Type II are aqueous inclusions. They occur in isolation and as clusters throughout single grains of white quartz together with aqueous–carbonic inclusions or in isolation and in clusters along mineral growth planes of transparent quartz, indicating a primary and/or pseudosecondary origin (Figs. 5d–f). Inclusions along healed cracks that cut across different quartz grains or euhedral quartz crystals have highly variable shapes and liquid:vapor ratios, and are considered secondary in origin (Fig. 5d). At room temperatures (25°C) they consist of two (liquid water-rich + vapor water = Type IIa) or three (liquid water-rich + vapor water + mica = Type IIb) phases (Figs. 5e, f and i), with vapor bubbles occupying 20 to 30 vol percent of the inclusions. Type IIa inclusions commonly occur as isolated inclusions or as clusters throughout a single grain or along mineral growth planes, and occur as continuous trails along healed cracks of white and transparent vein quartz. Type IIa inclusions from white quartz of the sericite-rich zone of vein margins are typically present as isolated aqueous inclusions, or coexist with type IIb and type I inclusions, indicating unmixing or boiling. These fluid inclusions have negative crystal, round, subround or irregular shapes and are generally <35 μm in maximum dimension. Type IIa inclusions from transparent quartz occur isolated or as clusters or trails coexisting with type IIb, and have negative crystal, subrounded or irregular shapes. These inclusions range in diameter from 2 to 60 μm. Type IIb inclusions occur dominantly as clusters coexisting with type IIa and type I inclusions throughout a single grain of white or

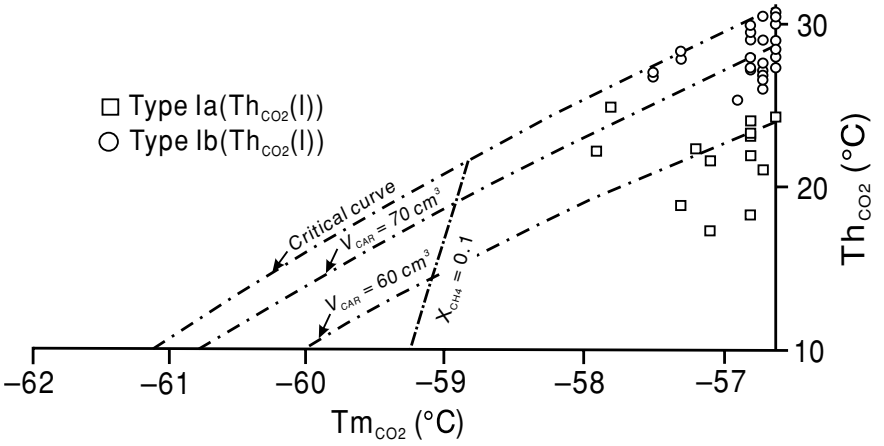

Fig. 6. Final melting temperature of CO_2 (Tm_{CO2}) versus homogenization temperature of CO_2 (Th_{CO2}) of type Ia and Ib inclusions from the Namseong deposit. Contours of mole fraction of CH_4 (X_{CH4}) and molar volume of carbonic phase (V_{CAR}), and critical curve constructed assuming homogenization to the liquid from figures in Thiéry et al. (1994) and Ridley and Hagemann (1999). Note the type Ia inclusions have lower Th_{CO2} values than type Ib, reflecting similar contents of CH_4 and lower densities. Also note the clustering by composition and molar volume, and the relatively narrow range of V_{CAR}.

transparent quartz. They have negative crystal or round shapes and range from 10 to 35 μm in diameter.

MICROTHERMOMETRY

More than 300 fluid inclusions in quartz have been studied by freezing and heating experiments, with freezing experiments performed first on all sections. The salinities of aqueous phases, mole fractions, and bulk density of type I and II inclusion were calculated using the MacFlinCor program (Brown and Hagemann, 1995) from equations of Diamond (1992) and Bodnar and Vityk (1994) and equations of state provided within the MacFlinCor program (Brown and Hagemann, 1995). The final melting temperature of CO_2 (Tm_{CO2}) was also measured to evaluate the purity of the CO_2 phase. Attempts were made to measure the homogenization temperature of the CO_2 (Th_{CO2}) during heating, in order to ascertain the density of CO_2, and the total homogenization temperature (Th_{total}). All errors are quoted at 1σ level.

Type I inclusions Upon cooling, an initial vapor bubble nucleated in the CO_2 phase within the temperature range –97°C to –93°C with an average of –96.0 ± 1.5°C (type Ia, –99°C to –95°C, average –97.5 ± 1.0°C (n = 9); type Ib, –99°C to –94°C, average –95.6 ± 1.4°C (n = 31)). The first melting temperature of the CO_2 phase lay in the range –87°C to –77°C with an average of –82.6 ± 3.1°C (type Ia, –87°C to –77°C, average –80.2 ± 3.3°C (n = 11); type Ib, –87°C to –78°C, average –83.4 ± 2.5°C (n = 29)). The final melting temperature of the CO_2 phase lay in the range –57.9°C to –56.6°C with an average of –56.8 ± 0.3°C (type Ia, –57.9°C to –56.6°C, average –57.0 ± 0.4°C (n = 16); type Ib, –57.5°C to –56.6°C, average –56.7 ± 0.2°C (n = 46)) (Table 1 and Fig. 6). These values are in part lower than or near the triple point for pure CO_2 (–56.6°C), from which it is deduced that very small concentrations of CH_4 or N_2 (Burruss, 1981; Shepherd *et al*., 1985). Type I inclusions all homogenized to a liquid (Th_{CO2}(l)) in a range from 17.3°C to 24.6°C with an average of 21.7 ± 2.2°C (n = 19) for type Ia inclusions and from 25.2°C to 30.9°C with an average of 28.5 ± 1.7°C (n = 49) for type Ib inclusions (Table 1 and Fig. 6). First and final melting temperatures of ice were very difficult to observe due to the small size of the inclusions and have not been recorded. In type I inclusions we observed the melting temperature of clathrate ($Tm_{clathrate}$) in the presence of both liquid and vapor CO_2, indicating that melting behaviour of these inclusions show the characteristics of typical Q_2 melting suggested by Diamond (1992) and Bakker (1997). The $Tm_{clathrate}$ values for type Ia and type Ib inclusions range from 8.6 to 10.8°C (average 9.3 ± 0.6°C, n = 17) and from 7.8 to 10.1°C (average 8.5 ± 0.6°C, n = 42), respectively (Table 1 and Fig. 7). Some type I inclusions with $Tm_{clathrate}$ values >10°C have Tm_{CO2} ranging from –57.8°C to –57.1°C (Fig. 7). They may result from a mixture of CO_2 and CH_4 clathrates ($CO_2 \cdot 5.75H_2O$ and $CH_4 \cdot 7H_2O$) (Hagemann *et al*., 1992; Yao *et al*., 2001). Collins (1979) suggested that $Tm_{clathrate}$ values of >10°C for H_2O–CO_2 inclusions indicate the presence of minor amounts of other volatiles such as CH_4 or N_2. In view of the indicated presence of CH_4 in some of type I inclusions, the salinities of the aqueous phase given represent minimum values. Using the computer program of Brown and Hagemann (1995) and the equation of Diamond (1992), the salinities of these inclusions are estimated to range from 0.0 to 4.3 wt.% NaCl equiv. with an average

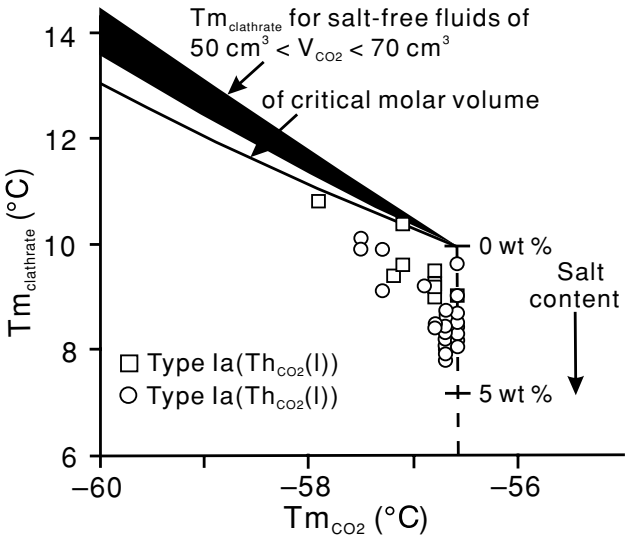

Fig. 7. Final melting temperature of clathrate ($Tm_{clathrate}$) versus final melting temperature of CO_2 (Tm_{CO2}) of type Ia and Ib inclusions from the Namseong deposit. The shaded area shows final melting temperature of clathrate and final melting temperature of CO_2 of salt-free H_2O–CO_2–CH_4 mixtures with carbonic molar volumes of the range shown from data in Seitz and Pasteris (1990). The Q_2 invariant clathrate melting point for the H_2O–CO_2–NaCl system is after Diamond (1994). Note the type Ib inclusions have lower $Tm_{clathrate}$ values than type Ia, reflecting higher contents of NaCl. Also note the clustering by sample with salinities of less than about 5 wt.% NaCl equiv. and the wide range of Tm_{CO2}, indicating the presence of variable amounts of CH_4.

of 2.5 ± 1.9 wt.% NaCl equiv. (type Ia, 0.0–2.8 wt.% NaCl equiv., average 1.5 ± 0.9 wt.% NaCl equiv. (n = 17); type Ib, 0.0–4.3 wt.% NaCl equiv., average 3.0 ± 1.1 wt.% NaCl equiv. (n = 42)) in the aqueous phase (Table 2 and Fig. 7). The true salinities of type I inclusions will be higher than those calculated (between 0.0 and 4.3 wt.% NaCl equiv.).

Type I inclusions generally decrepitate before total homogenization owing to internal pressures arising from their high CO_2 contents (Burruss, 1981). However, about 55 Th_{total} values were recorded from negative crystal or regular shaped inclusions by slow heating. Type I inclusions partly homogenized to the aqueous phase between 257°C and 354°C with an average of 315 ± 33°C (type Ia, 276–342°C, average 307 ± 24°C (n = 8); type Ib, 257–354°C, average 321 ± 38°C (n = 10)) and mostly to the CO_2 phase between 250°C and 380°C with an average of 314 ± 25°C (type Ia, 289–336°C, average 317 ± 17°C (n = 7); type Ib, 250–380°C, average 314 ± 26°C (n = 30)) (Table 1 and Fig. 8a).

Type II inclusions Initial ice melting for type II inclusions range from –25.9°C to –19.5°C with an average of

Table 2. Summary of compositions, molar volumes, and densities of fluid inclusions from the Namseong deposit

Inclusion	Bulk inclusion composition				Carbonaceous phase composition		Aqueous phase composition	Molar volume	Density (g/cm^3)	
	X_{H2O}	X_{NaCl}	X_{CO2}	X_{CH4}	X_{CO2}	X_{CH4}	Eq.wt.% NaCl	V_{bulk}	d_{CO2}	D_{bulk} (d_{H2O})
Type Ia	0.26–0.82	0.00–<0.01	0.17–0.73	0.00–0.01	0.96–1.00	0.00–0.04	0.0–2.8	24.9–49.6	0.64–0.79	0.75–0.91
	(0.55 ± 0.23)	(0.002 ± 0.002)	(0.44 ± 0.24)	(0.01 ± 0.004)	(0.98 ± 0.01)	(0.02 ± 0.01)	(1.5 ± 0.9)	(37.0 ± 10.1)	(0.73 ± 0.04)	(0.82 ± 0.06)
Type Ib	0.28–0.85	0.00–0.01	0.14–0.72	0.00–<0.01	0.97–1.00	0.00–0.03	0.0–4.3	28.4–54.9	0.53–0.70	0.63–0.85
	(0.54 ± 0.20)	(0.005 ± 0.002)	(0.46 ± 0.20)	(0.002 ± 0.003)	(0.99 ± 0.01)	(0.01 ± 0.01)	(3.0 ± 1.1)	(42.2 ± 9.4)	(0.62 ± 0.06)	(0.73 ± 0.06)
Type IIa	0.98–1.00	0.00–0.02					0.0–7.0	18.8–26.1		0.72–0.96
	(0.99 ± 0.01)	(0.01 ± 0.01)					(2.2 ± 1.9)	(22.1 ± 1.6)		(0.83 ± 0.05)
Type IIb	0.98–1.00	0.00–0.02					0.4–5.6	19.0–22.6		0.83–0.95
	(0.99 ± 0.01)	(0.01 ± 0.01)					(2.7 ± 1.6)	(21.2 ± 1.2)		(0.87 ± 0.04)

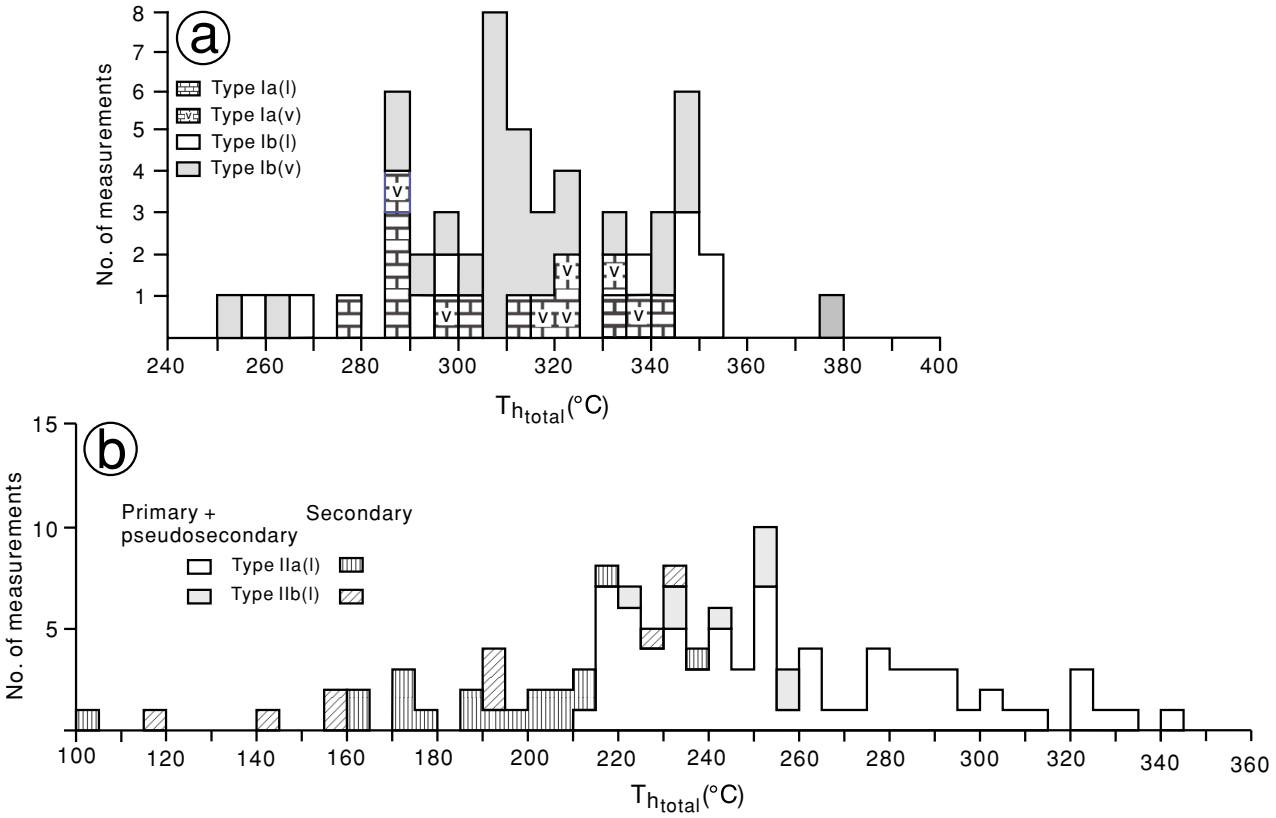

Fig. 8. a) Frequency histogram of total homogenization temperature (Th_{total} (°C)) of type I inclusions from the Namseong deposit. b) Frequency histogram of total homogenization temperature (Th_{total} (°C)) of type II inclusions from the Namseong deposit. Note type I and II inclusions plot near the 310°C and 250°C homogenization temperature, respectively.

–23.6 ± 1.6°C (type IIa, –25.9°C to –19.5°C, average –23.7 ± 1.7°C (n = 35); type IIb, –25.1°C to –22.3°C, average –23.5 ± 1.1°C (n = 6)), indicating that these inclusions mainly contain cations such as Na^+ and K^+ in the liquid phase (Davis *et al*., 1990). The Tm_{ice} values for type II inclusions range from –4.4°C to 0°C with an average of –1.5 ± 1.2°C (type IIa, –4.4°C to 0°C, average –1.4 ± 1.2°C (n = 97); type IIb, –3.4°C to –0.5°C, average –2.2 ± 0.9°C (n = 9)) for primary inclusions, and from –1.6°C to –0.2°C with an average of –0.8 ± 0.4°C (n = 25) for secondary inclusions (Table 1). Using the computer program of Brown and Hagemann (1995), and equation of Bodnar and Vityk (1994), the salinities are estimated to be 0.0–7.0 wt.% NaCl equiv. with an average of 2.5 ± 1.9 wt.% NaCl equiv. (type IIa, 0.0–7.0 wt.% NaCl equiv., average 2.4 ± 1.9 wt.% NaCl equiv. (n = 97); type IIb, 0.9–5.6 wt.% NaCl equiv., average 3.7 ± 1.5 wt.% NaCl equiv. (n = 9)) for primary inclusions and 0.4–2.7 wt.% NaCl equiv. with an average of 1.4 ± 0.8 wt.% NaCl equiv. (n = 25) for secondary inclusions (Table 2). Type II inclusions all homogenized to a liquid phase at temperatures ranging from 195°C to 342°C with an average of 257 ± 33°C (type IIa, 195–342°C, average 258 ± 34°C (n = 73); type IIb, 225–260°C, average 246 ± 12°C (n = 9)) for primary inclusions and from 104°C to 230°C with an average of 187 ± 32°C (n = 28) for secondary inclusions (Table 1 and Fig. 8b).

Stable Isotope Studies

Samples of quartz veins from underground stopes were collected for stable isotope study. Pyrite and quartz crystals were crushed and selected from macroscopically homogenous portions. Pyrite and quartz separates were obtained by handpicking under a binocular microscope. For $\delta^{34}S$ analyses, SO_2 was produced from pyrite and reacted with CuO at 1000°C. Quartz selected for $\delta^{18}O$ analyses was reacted at 650°C with BrF_5 in nickel vessels to liberate oxygen and then converted to CO_2 by reaction with an internally heated carbon rod (Clayton and Mayeda, 1963). Although the water for δD analysis was released from fluid inclusions by new coupling vacuum techniques with either crushing/milling or thermal decrepitation (Simon, 2001; Dallai *et al*., 2004; Baatartsogt *et al*., 2007;

Table 3. Sulfur, oxygen and hydrogen isotopic data of minerals from the Namseong deposit

Sample number	Mineral	$\delta^{34}S$ (‰)	$\delta^{18}O$ (‰)	$\delta^{34}S_{H2S}$ (‰)[1]	$\delta^{18}O_{H2O}$ (‰)[2]	δD (‰)	$\Delta^{34}S$	T (°C)[3]	Th (°C)[4]
NS sample5	Pyrite (wallrock)	7.1		6.1					350
NS87817	Pyrite (wallrock)	8.0		7.0					350
NS87817	Pyrite	5.2		3.7					250
NS4	Pyrite	6.8		5.3					250
NS87319-1	Pyrite	7.7		6.2					250
NS12-1	Pyrite	5.8		4.3					250
NS17	Pyrite	5.9		4.4					250
NS87319-1	Sphalerite	7.6		7.2					250
NS97319-1	Pyrite	7.8		6.3					250
NS12	Pyrite	7.1		5.6			Py–Sp		250
NS12	Sphalerite	6.0		5.6			1.1	251	250
NS sample5	Transparent quartz		4.8		–0.5	–75			350
NS87817	Transparent quartz		5.6		0.3	–83			350
NS4	White quartz		6.7		1.4	–83			350
NS87319-1	Transparent quartz		3.7		–1.6	–70			350
NS97319-1	White quartz		3.1		–2.2	–68			350
NS12	Transparent quartz		6.9		1.6	–78			350
NS12	White quartz		6.2		0.9	–77			350
NS5	Transparent quartz		4.6		–0.7	–64			350
NS17	White quartz		6.4		1.1	–68			350

[1] *$\delta^{34}S_{H2S}$ (‰) is calculated from the equatin by Ohmoto and Rye (1979).*
[2] *$\delta^{18}O_{H2O}$ (‰) is calculated from the equation given by Matsuhisa et al. (1979).*
[3] *Isotopic temperature calculated from fractionation factors given by Ohmoto and Rye (1979).*
[4] *Th (°C) is homogenization temperature of fluid inclusions.*

Verheyden *et al*., 2008; Dublyansky and Spötl, 2009), there are some doubts as to the usefulness of δD analyses values determined from fluid inclusions in vein quartz (Faure *et al*., 2002; Faure, 2003; Harris *et al*., 2005). However, we are confident that the analyzed results are not mixed isotopic compositions because of careful sample selection and separation. Quartz separates were outgassed under high-vacuum at 180°C in order to remove the surface absorbed water and the water of secondary inclusions. Water for δD determinations was extracted from fluid inclusions in quartz by thermal decrepitation at 500°C under vacuum. The extracted water was reduced to hydrogen by reaction with zinc metal at 450°C (Coleman *et al*., 1982). The sulfur, oxygen and hydrogen isotopic compositions of pyrite and quartz were determined on a Finnigan-MAT251 mass spectrometer. Data are reported in standard δ notation relative to the troilite in Canyon Diablo meteorite (CDT) standard for S and the Vienna SMOW for O and H. The standard errors of each analysis are approximately ±0.2 per mil for S and O, and ±2 per mil for H. All uncertainties are reported here at 1σ level.

Sulfur, Oxygen and Hydrogen Isotope Data

Sulfur isotope analyses were performed on 11 monomineralic samples from the Namseong underground stopes (Table 3). The $\delta^{34}S$ values of pyrite range from 5.2‰ to 8.0‰ with an average of 6.8 ± 1.0‰ (n = 9). The $\delta^{34}S$ values of pyrite from the wall-rock alteration zone are higher than those of pyrite from the quartz veins, but no temporal, spatial or vertical variation in $\delta^{34}S$ values was observed (Table 3). The $\delta^{34}S$ values of sphalerite range from 6.0‰ to 7.6‰ with an average of 6.8 ± 1.1‰ (n = 2). A pyrite-sphalerite pair that exhibited textures of coprecipitation has $\Delta^{34}S$ values of 1.1‰ and yield equilibration isotopic temperatures of 251 ± 30°C (Ohmoto and Rye, 1979), in agreement with the fluid inclusion homogenization temperatures in associated quartz.

The $\delta^{18}O$ values of 4 white and 5 transparent quartz samples from the Namseong underground stopes range from 3.1‰ to 6.7‰ with an average of 5.6 ± 1.7‰ (n = 4) and from 3.7‰ to 6.9‰ with an average of 5.1 ± 1.2‰ (n = 5), respectively (Table 3). No temporal, spatial or vertical variation in $\delta^{18}O$ values was observed. Using the quartz-water isotope fractionation equation of Matsuhisa *et al*. (1979), coupled with the measured fluid inclusion temperatures, the calculated $\delta^{18}O$ values of water from the quartz samples range from –2.2‰ to 1.4‰ with an average of 0.3 ± 1.7‰ (n = 4, white quartz) and from –1.6‰ to 1.6‰ with an average of –0.2 ± 1.2‰ (n = 5, transparent quartz), respectively (Table 3). The δD_{SMOW} values of the extracted waters for the same nine quartz samples range from –83‰ to –68‰ with an average of

–74.0 ± 7.3‰ (n = 4) and –83‰ to –64‰ with an average of –74.0 ± 7.3‰ (n = 5), respectively (Table 3).

Discussion

Quantitative estimation of fluid composition and density

Two hydrothermal fluids appear to be contained in the quartz samples of the only one stage veins of the Namseong deposit: an early aqueous–carbonic fluid with minor CH_4 and a later aqueous fluid. The early fluid is represented by coexisting minor CO_2–H_2O inclusions and mainly aqueous inclusions that unmixed from a single parent fluid. The late fluid is represented by the primary aqueous inclusions that originated by mixing with circulating meteoric water.

Most type I inclusions have Tm_{CO2} values below or near –56.6°C, which are interpreted to result from the presence of other species such as CH_4 and N_2 (Burruss, 1981). All type I inclusions exhibit the same phase behavior as H3-type described by Van den Kerkhof and Thiéry (1994, 2001). Plots of the low-temperature behavior of the CO_2 phases (Tm_{CO2} and Th_{CO2}) of type I inclusions are presented in Fig. 8a. It shows that some inclusions with no CH_4 have high density. A volume versus X_{CH4} projection in the CO_2–CH_4 system allows the relative proportions of CH_4 and CO_2 present in the CO_2 phases of type I inclusions to be estimated using the computer program of Brown and Hagemann (1995), and the graphs of Thiéry *et al*. (1994), assuming that CH_4 is the only additional component present. The approximate X_{CH4} values of the CO_2 phases estimated from the Tm_{CO2} and Th_{CO2} values of the type I inclusions are listed in Table 2. The calculated X_{CO2} values for these inclusions are also given.

The bulk densities and chemical compositions of type I and type II inclusions were calculated from microthermometric and volumetric data using the computer program of Brown and Hagemann (1995). In order to estimate the bulk composition of type I inclusions, the volume ratio of CO_2 to H_2O must be determined. The mole percent CO_2 of carbonic–aqueous inclusions can be ascertained from Th_{CO2}, $Tm_{clathrate}$, and Th_{total}, and the mole percent CO_2 can then be converted to the volume percent CO_2. The calculated total density values for these inclusions are listed in Table 2. It is noteworthy that the calculated fluid density generally increases from type I inclusions to type II inclusions (Table 2), probably indicating that trapping of fluid inclusions followed this same order with a progressive increase in fluid density from the early to the late stage of mineralization. In summary, the parental fluids that deposited quartz at Namseong had approximate salinities of <4.3 wt.% NaCl equiv., X_{CO2} + X_{CH4} contents of 0.12 to 0.74, and total densities of 0.63–0.91 g/cm^3, and the fluids evolved toward H_2O-rich compositions with less than about 7.0 wt.% NaCl equiv. and total densities ranging from 0.72 to 0.96 g/cm^3 by partly unmixing and mainly mixing with meteoric water through the paragenetic sequence.

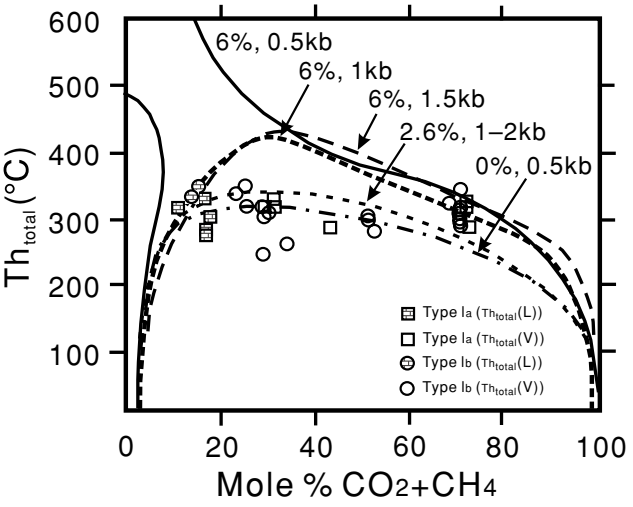

Fig. 9. Total homogenization temperature (Th_{total} (°C)) versus calculated equivalent mole fraction CO_2 + CH_4 of type I inclusions from the Namseong deposit. The curves for 0–6 wt.% NaCl are modified from Hendel and Hollister (1981), Bowers and Helgeson (1983), and Brown (1998). Note most type I inclusions plot on or near the solvus curve for H_2O–CO_2-0 and 6 wt.% NaCl at 0.5 and 1 kbar at temperatures of 250°C to 350°C.

Fluid unmixing and mixing, and its implications for gold and silver mineral precipitation

There are many lines of evidence for immiscibility as a mechanism responsible for producing fluids observed in some inclusions (Ramboz *et al*., 1982; Roedder, 1984; Diamond, 2001; Van den Kerkhof and Hein, 2001; Hagemann and Lüders, 2003). Early white quartz veins with wall-rock alteration contain abundant aqueous–carbonic inclusions coexisting with aqueous inclusions in clusters and are interpreted to have been trapped contemporaneously and to have originated by fluid unmixing. The carbonic volume % of type I inclusions ranges from 30–40% to 90% and CO_2-rich inclusions are vastly more abundant than water-rich inclusions. CO_2-rich and water-rich type I inclusions undergo total homogenization in the same temperature range (Fig. 9). For example, type I inclusions either homogenized to the aqueous phase between 257°C and 354°C (average 315 ± 33°C, n = 18) or homogenized to the CO_2 phase between 250°C and 380°C (average 314 ± 25°C, n = 37) (Table 1). Type I inclusions in a single cluster (FIA) either homogenized to the aqueous phase between 257°C and 352°C (average 315 ± 40°C, n = 8) or to the CO_2 phase between 250°C

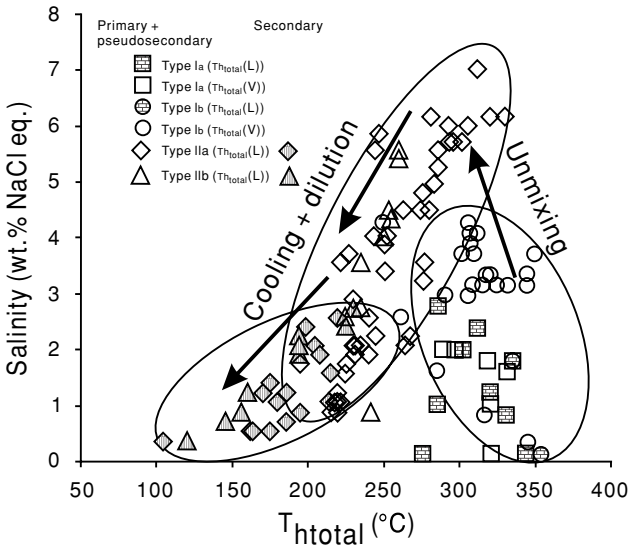

Fig. 10. Salinity versus total homogenization temperature diagram for type I and II inclusions from the Namseong deposit. Type I inclusions from early stage represent unmixing of a low salinity H_2O–CO_2 fluid, but type II inclusions are later inclusions with low salinities. Note most type II inclusions display a trend of decreasing salinity with decreasing total homogenization temperature.

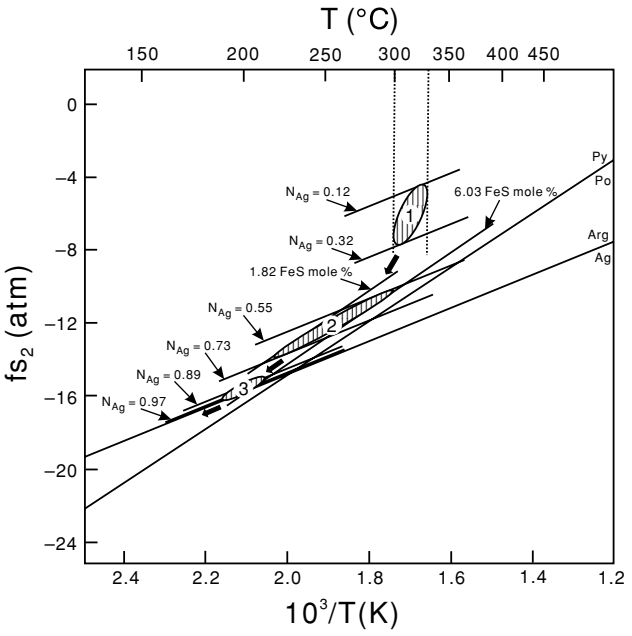

Fig. 11. Temperature versus sulfur fugacity (f_{S2}) diagram showing the ranges of gold and silver depositional conditions indicated by mineral assemblages from the Namseong deposit. Ranges of temperature and f_{S2} were estimated from phase relations, mineral compositions in the systems Fe–Zn–S (Barton and Skinner, 1979), Au–Ag–S (Barton and Toulmin, 1964), and total homogenization temperatures. Field 1 represents coexisting electrum (12.05–31.59 at.% Ag), pyrite and quartz (homogenization temperature of type II inclusions, 300–330°C). Field 2 represents coexisting electrum (55.28–73.49 at.% Ag), pyrite, sphalerite (1.82–6.03 mole% FeS), chalcopyrite, galena and argentite. Field 3 represents electrum (82.03–97.24 at.% Ag), argentite, pyrargyrite and native silver in late stage. N_{Ag}, atomic fraction of silver in electrum; FeS mole %, mole fraction of FeS in sphalerite; Ag, native silver; Arg, argentite; Po, pyrrhotite; Py, pyrite.

and 380°C (average 313 ± 27°C, n = 24). Most type I inclusions plot along or close to the solvus for fluids with 0 and 6 wt.% NaCl at 0.5–1 kbar (Fig. 9). Unmixing of H_2O–CO_2–NaCl fluids between these solvi at temperatures of 300°C to 400°C would produce CO_2-rich fluids (X_{CO2} values > 0.56) such as those observed in the Namseong deposit. Results such as these are generally regarded as convincing evidence for fluid unmixing (Roedder, 1984; Hagemann and Lüders, 2003).

Many type I inclusions fall into the high X_{CO2} compositional type defined by Diamond (2001), suggesting that they originated by unmixing or boiling. Van den Kerkhof and Hein (2001) suggested that trapping of a homogeneous fluid by phase separation after cooling may result in fluid inclusions of similar appearance, composition and density. However, trapping of heterogeneous fluids or during boiling may result in fluid inclusions of variable composition and density (Van den Kerkhof and Hein, 2001). The microthermometric data of type I inclusions indicate that the fluid was trapped homogeneously.

Type II inclusions coexisting with type I inclusions have high salinities (1.9–7.0 wt.% NaCl with an average of 4.9 ± 1.6 (n = 15)) and homogenization temperatures (255–343°C with an average of 295 ± 25°C (n = 18)). Although some of the variation can be attributed to analytical errors, homogeneous trapping of immiscible fluids can also produce similarity in phase relations, in homogenization temperatures, and in compositions of simultaneously-trapped fluid inclusions (Ramboz *et al.*, 1982). Type II inclusions have higher salinities and lower homogenization temperatures than those of type I inclusions (Fig. 10); this is consistent with fluid unmixing (Roedder, 1984; Coulibaly *et al.*, 2008). Type II inclusions in transparent quartz are found as primary, pseudosecondary in growth planes, or secondary inclusions in healed fractures and were not found to be associated intimately with type I inclusions. Type II inclusions display a trend of decreasing salinity with decreasing temperature (Fig. 10). This may indicate later cooling and dilution of ore fluids, probably as a result of mixing with deeply circulating meteoric waters. If this is correct, the majority of aqueous type II inclusions may be unrelated to the early fluid unmixing within the hydrothermal sys-

tem. Therefore, we conclude that the aqueous inclusions represent fluids that evolved through unmixing of H_2O–NaCl–CO_2 fluids or that evolved by mixing of fluids from different sources.

Gold in hydrothermal fluids is mostly transported as gold hydrosulfide, chloride and hydroxy complexes (Shenberger and Barnes, 1989; Hayashi and Ohmoto, 1991; Benning and Seward, 1996; Stefánsson and Seward, 2003, 2004). Experimental studies have demonstrated that gold is soluble as hydrosulfide complexes at low salinities and low f_{O2} but at variable pH conditions. The $Au(HS)_2^-$ complex is predominant in near neutral to weakly acidic pH reduced sulfur-bearing fluids with relatively low temperatures (Renders and Seward, 1989; Shenberger and Barnes, 1989; Benning and Seward, 1996; Stefánsson and Seward, 2003; Tagirov *et al*., 2005), whereas the AuHS° and $HAu(HS)^\circ_2$ complexes are stable under acidic fluids (Seward, 1973; 1989; Shenberger and Barnes, 1989; Gibert *et al*., 1998). The chloride complex of gold is predominant in more acidic and high salinity H_2S-poor fluids at relatively high f_{O2} (Stefánsson and Seward, 2003). The hydroxy complex of gold is predominant in strongly alkaline and reduced fluids (Stefánsson and Seward, 2003).

The initial pH of hydrothermal fluids for the Namseong deposit is constrained by the mineral association with sericite and silicic alteration. Lack of calcite suggests pH to be between 5.2 (microcline–sericite equilibrium) and 6.2 (calcite saturation) based on fluid inclusion data (315°C, 2.5 wt.% NaCl equiv.). The f_{O2} values can be estimated from the chemical equilibria ($CH_4 + 2O_2 = CO_2 + 2H_2O$, $3C + O_2 + 2H_2O = 2CO_2 + CH_4$) of the C–H–O system reported by Holloway (1981) and fluid inclusion data, as 10^{-30} atm and 10^{-38} atm at 354°C and 250°C respectively. The presence of pyrite and the lack of sulfate minerals and hematite indicate that the fluids were reduced. It would therefore seem likely that gold was dominantly transported as $Au(HS)_2^-$ complex in the ore-forming fluids.

Gold deposition from the $Au(HS)_2^-$ complex may be caused by several mechanisms (Seward, 1984; Cole and Drummond, 1986; Hayashi and Ohmoto, 1991; Benning and Seward, 1996; Gibert *et al*., 1998). These include 1) pH change from near-neutral to more acidic or alkaline conditions, 2) change in f_{O2} from redox reactions and/or CO_2 immiscibility, 3) decrease in the activity of reduced sulfur species as a result of sulfide precipitation, wall-rock alteration, and/or H_2S loss accompanying fluid unmixing, and 4) cooling and dilution of ore-forming fluids. A change in pH at Namseong deposit would not have been an effective cause of gold deposition because the gold occurs as inclusions in pyrite or as fracture fillings accompanying sphalerite, chalcopyrite, and galena. A decrease in fluid f_{O2} may well have occurred as a result of interactions with the wall-rocks, albeit limited, and thus caused a reduction in $Au(HS)_2^-$ activity.

The variation in fs_2 and temperature of hydrothermal fluids was estimated by examining available mineral assemblages based on chemical compositions of sphalerite and electrum and fluid inclusion data (Fig. 11). Electrum (12.05–31.59 at.% Ag) is closely intergrown with pyrite and quartz (homogenization temperature of type II inclusions, 300–330°C), which indicates approximate depositional log fs_2 values of –4.4 to –7.8 atm for pyrite and electrum (Field 1 in Fig. 11). Electrum (55.28–73.49 at.% Ag) is closely intergrown with pyrite, sphalerite (1.82–6.03 mole% FeS), chalcopyrite, galena and argentite, which indicates that the ore minerals were deposited in the temperature range 212–312°C and log fs_2 values of –9.8 to –14.2 atm (Field 2 in Fig. 11). The composition of electrum (82.03–97.24 at.% Ag), and the presence of argentite, pyrargyrite and native silver in late stage indicate that economic minerals were deposited at a temperature of <240°C and log fs_2 values of <–14.2 atm (Field 3 in Fig. 11).

Fluid inclusions in white and transparent quartz show evidence of partial fluid unmixing and mainly cooling and dilution resulting from mixing with meteoric water during mineralization. Therefore, we suggest that deposition of early wall-rock alteration minerals and base metal sulfides resulted in loss of H_2S and changes in pH and f_{O2} associated with unmixing, and then economic minerals such as electrum and silver minerals were deposited by destabilization of a gold hydrosulfide complex as a result of a decrease in sulfur fugacity/aH_2S/aCl, oxygen fugacity and temperature that accompanied sulfide precipitation from the aqueous fluid during cooling and dilution.

Pressure-temperature-depth conditions during mineralization

Isochores were calculated for type I inclusions using the FLUIDS program (Bakker, 2003) and the data of Bowers and Helgeson (1983) and Bakker (1999), which are in close agreement with lines of constant homogenization temperature predicted by the equation of state of Duan *et al*. (1996). For type II inclusions, isochores were calculated with the MacFlinCor program (Brown and Hagemann, 1995) using the data of Bodnar and Vityk (1994). In this case, trapping temperatures were estimated from the results of the fluid inclusion study and sulfur stable isotope thermometry and principal methods for calculating pressures are based on 1) the intersecting fluid isochors for coeval fluids, and 2) fluid isochores used in conjunction with independent geothermometers (Shepherd *et al*., 1985). The isochores were plotted using the lower and upper densities of type I and type II inclusions (Fig. 12).

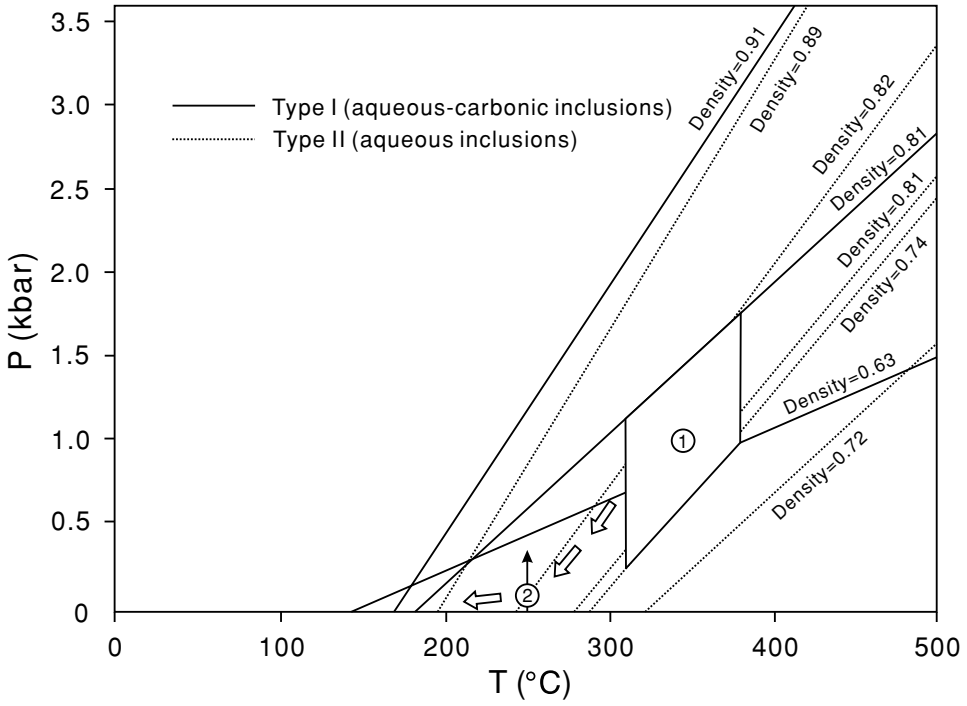

Fig. 12. Pressure and temperature diagram displaying isochores of the minimum and maximum densities of the two types of fluid inclusions from the Namseong deposit. Field 1 represents coexisting types I and II inclusions from white quartz. Field 2 represents average value of type II inclusions from white and transparent quartz.

The highest homogenization temperature of 380°C for type I inclusions coexisting with type II inclusions from the early stage provides a minimum temperature for the original trapping conditions. At this temperature (380°C) and average temperature (310°C) of type I and II inclusions, the isochores of the type I and II inclusions indicate a pressure range from 260–1,700 bars; most of the data are distributed from 700 to 1,300 bars (Field 1 in Fig. 12). These values correspond to minimum formation depths between 2.5 and 4.7 km for lithostatic conditions.

The Th_{total} values of the immiscible type I and II inclusions are interpreted to correspond to their trapping temperatures. Most type I inclusions fall between the solvus for H_2O–CO_2–0 wt.% NaCl or H_2O–CO_2–6 wt.% NaCl at 0.5–1 kbar at temperatures of 300°C to 350°C (Bowers and Helgeson, 1983; Brown, 1998) (Fig. 9). The availability of an independent geothermometer provided more precise calculation of the trapping pressure of the type II inclusions from white and transparent quartz of late stage (Rios *et al*., 2003). The average density of type II inclusions and the pyrite–sphalerite geothermometer (251°C) makes it possible to set *P*–*T* constraints. At this temperature, the entrapment pressure of those inclusions is 100 bars (Field 2 in Fig. 12), suggesting minimum formation depth of 1.0 km for hydrostatic conditions.

Possible sources and evolution of ore-forming fluids

Cretaceous deposits such as Yonghwa (96 Ma), Weolseong (96 Ma), Soowang (96 Ma) and Weolyu (79 Ma), occur in the Seolcheon metallogenic province and are related to Cretaceous igneous activity (Youn and Park, 1991, 1993, 1997; Yun *et al*., 1993). Youn and Park (1991, 1993, 2004) reported that sericite from the Yonghwa, Weolseong and Soowang deposits yielded K–Ar ages of 96 Ma, indicating a middle Cretaceous age for gold and silver mineralization, probably related to intrusion of porphyritic granite (98.7 ± 3.6 Ma; K–Ar on biotite). Yun *et al*. (1993) reported that the K–Ar age of sericite from the Weolyu deposit is 79 Ma, indicating a late Cretaceous age for the Weolyu gold and silver mineralization, probably associated with intrusion of quartz porphyry (81.5 ± 1.8 Ma; K–Ar on wall-rock) (Table 4).

The gold mineralization in the Namseong deposit occurred at 78 Ma, indicating that the gold mineralization in this deposit is related to late Cretaceous igneous activity (Sogrisan granite: 91 Ma by whole rock Rb–Sr or 72 Ma by K–Ar on biotite; quartz porphyry: 82 Ma using whole rock K–Ar; Yun and Kim, 1990; Cheong and Chang, 1997; Ree *et al*., 2001).

The Sogrisan granite contains miarolitic cavities and pegmatitic pockets, and euhedral quartz, alkali feldspar

Table 4. Characteries of some deposits from the Seolcheon Metallogenic Province

Deposits	Namseong	Yonghwa	Weolseong	Weolyu	Soowang (Narim)
	Au–Ag	Au–Ag	Au–Ag	Au–Ag	Au–Ag
Age	Cretaceous (78 Ma)	Cretaceous (96 Ma)	Cretaceous (96 Ma)	Cretaceous (79 Ma)	Cretaceous (96 Ma)
Vein direction	N20–30°W/70–85°SW	N15–25°W/70–85°SW	N5–25°W/85°SW	N10–65°E/65°NW	N35–40°W/80°NE
Depth of formation (m)	3,600 (early stage: 1,000 bar), 360 (late stage: 100 bar)	690 (180 bar) based on boiling (L_{H2O}–V_{H2O})	840 (220 bar) based on boiling (L_{H2O}–V_{H2O})	840 (early stage: 220 bar), 120 (late stage: 33 bar) based on boiling (L_{H2O}–V_{H2O})	800 (210 bar) based on boiling (L_{H2O}–V_{H2O})
Petrology of host units	Granite	Granite, gneiss	Granite, gneiss	Quartz porphyry, tuff, tuffaceous sandstone	Granite, gneiss
Hydrothermal alteration	Sericitization, silicification, pyritization, chloritization	Sericitization, chloritization	Sericitization, chloritization	Sericitization, silicification, pyritization, chloritization	Sericitization, chloritization, carbonitization
Mineralized vein type	Fissure-filling quartz veins	Fissure-filling quartz veins	Fissure-filling quartz veins	Fissure-filling quartz veins	Fissure-filling quartz veins
Vein mineralogy					
Silicate, carbonate minerals	Qtz–fl–cc	Qtz–an–cc	Qtz–sid–an–ba–cc	Qtz–fl–an–rho–cc	Qtz–sid–an–ba–cc
Ore minerals	Py–sp (1.8–6.0 mole% FeS)–cp–gn–el (2.8–88.0 at.% Au)–arg–pyr–si	Mag–ha–ru–py–po–asp (29.1–30.3 at.% As)–ma–sp (0.4–20.7 mole% FeS)–cp–gn–el (11.9–79.0 at.% Au)–arg–fre–pol–jal–mia–pyr–si	Mag–ha–ru–py–po–asp (29.1–30.4 at.% As)–ma–sp (0.9–11.5 mole% FeS)–cp–gn–el–arg–fre–pol–jal–mia–pyr–bou–si0	Ru–py–sp (0.9–5.9 mole% FeS)–cp–gn–el (3.4–48.3 at.% Au)–arg–pol–tetra–pro–ste–argy–si	Mag–ha–ru–py–po–asp (28.3–32.5 at.% As)–ma–sp (0.1–18.7 mole% FeS)–cp–gn–el (29.5–55.2 at.% Au)–arg–fre–pyr–bou–si
Ore grades	4–5 g/t Au, 120–125 g/t Ag	10 g/t Au	10.9 g/t Au, 10.8 g/t Ag	7.0 g/t Au, 600 g/t Ag	6.0 g/t Au, 116 g/t Ag
Ore reserves		15,300 M/T	58,300 M/T	25,000 M/T	10,270 M/T
Fluid inclusion					
Fluid system	H_2O–NaCl ± CO_2	H_2O–NaCl ± CO_2	H_2O–NaCl	H_2O–NaCl	H_2O–NaCl
Type	Type IIa > Type IIc > Type Ib > Type Ia	Type IIa > Type IIb > Type Ib	Type IIa > Type IIb	Type IIa > Type IIb > Type IIc	Type IIa > Type IIb
Th_{total} (°C)	104–380 (qtz)	162–312 (qtz), 132–173 (cc)	166–319 (qtz)	98–368 (qtz, sp, fl, an, cc)	117–329 (qtz, sid, sp, ba)
wt.% NaCl equiv.	0.0–7.0	0.3–6.9 (qtz), 1.0–4.2 (cc)	1.1–7.9	0.0–7.0	1.8–10.4
Stable isotope data (‰)					
Sulfur (calculated $\delta^{34}S_{H2S}$)	5.2–8.0 (3.7–7.2)	3.3–4.5	1.7–5.1	3.2–7.3 (3.0–6.0)	0.9–5.5
Oxygen (calculated $\delta^{18}O_{H2O}$)	Qtz: 3.1–6.9 (–2.2 to 1.6)	Qtz: 5.5 (–5.6 to –3.0), cc: 9.9–14.0 (–0.9 to 1.0), se: 3.9	Cc: 15.9 (1.9)	Qtz: 1.5–4.1 (–6.5 to –2.8), cc: –0.6 to 13.9 (–8.7 to 3.8)	Qtz: 4.2–7.1 (–9.3 to –2.0), cc: 17.0 (2.3), se: 8.3
Hydrogen (calculated δD_{H2O})	Qtz: –83 to –64	Se: –93		Qtz: –83 to –77, cc: –90 to –80	Se: –89.8
Carbon (calculated $\delta^{13}C_{H2CO3}$)		Cc: –4.2 to –3.5, an: –4.5	Cc: –3.7	Cc: –5.0 to –2.0	Cc: –8.7, sid: –6.5
Source of ore-forming fluids	Meteoric water	Meteoric water	Meteoric water	Meteoric water	Meteoric water
Ore deposition mechanism	Mixing, partly unmixing	Mixing, partly boiling	Mixing, partly boiling	Mixing, partly boiling	Mixing, partly boiling
Associated granitoids	Sogrisan granite or quartz porphyry (?)	Porphyritic granite (99 Ma)	Porphyritic granite (99 Ma)	Quartz porphyry (82 Ma)	Porphyritic granite (99 Ma)
Reference	This study	Youn and Park (1991, 1997)	Youn and Park (1993, 1997)	Yun *et al.* (1993); Lee *et al.* (1994)	Youn and Park (1997, 2004)

Type Ia, L_{H2O}–L_{CO2} (or V_{CO2}) inclusion; Type Ib, L_{H2O}–L_{CO2}–V_{CO2} inclusion; Type IIa, L_{H2O}-rich–V_{H2O} inclusion; Type IIb, L_{H2O}–V_{H2O}-rich inclusion; Type IIc, L_{H2O}-rich–V_{H2O}-solid inclusion. An, ankerite; Arg, argentite; Argy, argyrodite; Asp, arsenopyrite; Ba, barite; Bou, bournonite; Cc, calcite; Ch, chlorite; Cp, chalcopyrite; El, electrum; Fl, fluorite; Fre, freibergite; Gn, galena; Ha, hematite; Jal, jalpaite; Ma, marcasite; Mag, magnetite; Mia, miargyrite; Po, pyrrhotite; Pol, polybasite–pearceite; Pr, prehnite; Pro, proustite; Py, pyrite; Pyr, pyrargyrite; Qtz, quartz; Rho, rhodochrosite; Ru, rutile; Se, sericite; Si, native silver; Sid, siderite; Sp, sphalerite; Ste, stephanite; Tetra, argentian tetrahedrite–tennantite.

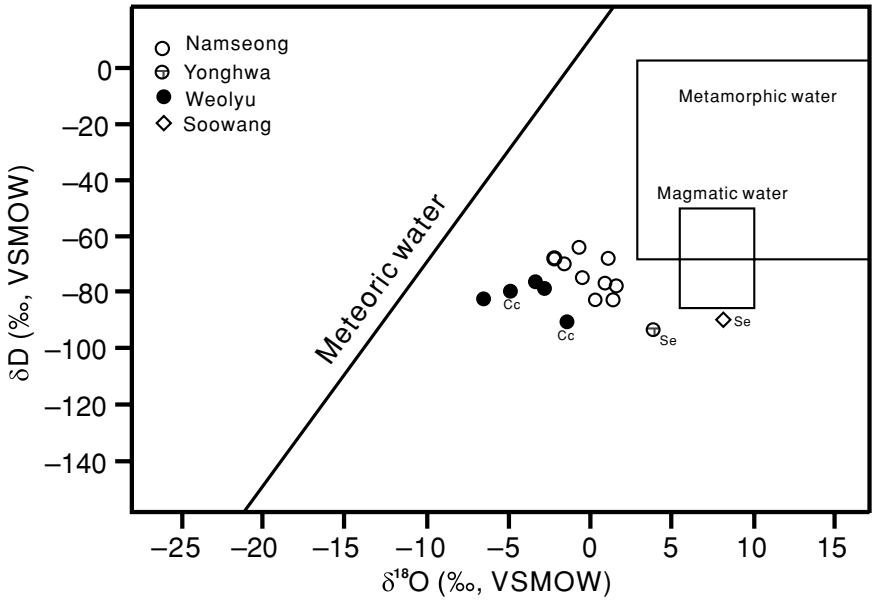

Fig. 13. Hydrogen versus oxygen isotope diagram showing calculated stable isotope hydrothermal fluid compositions from the Namseong deposit. Note data from the Yonghwa, Weolyu and Soowang deposits are interpreted to indicate meteoric water (Yun et al., 1993; Youn and Park, 1997), but some calculated $\delta^{18}O_{water}$ values of sericite from Yonghwa and Soowang deposits may be consistent with a magmatic origin. The primary magmatic and metamorphic water boxes are from Taylor (1979) and Sheppard (1986). Cc, calcite; Se, sericite.

and rarely calcite occur in the cavities (Lee *et al*., 2010). Lee *et al*. (2010) suggested that the Sogrisan granite is strongly fractionated and has related hydrothermal ore deposition; the peraluminous character of this granite can be interpreted to result from the removal of feldspar from the granitic melt (Chappell, 1999; Jwa, 2004; Lee *et al*., 2010). Cho *et al*. (1994) suggested that the Sogrisan granite was emplaced at a shallow level and rapidly crystallized from a magnetite-series magma. Sagong *et al*. (2001) suggested that the quartz porphyry may be the highly fractionated product of a felsic magma at the last stage of magmatic evolution. Thus textural features support the temporal and spatial evidence that indicates that the mineralization at the Namseong deposit is related to the Cretaceous Sogrisan granite or quartz porphyry.

The hydrothermal fluids of the Namseong deposit were $H_2O \pm CO_2$-bearing fluids with low salinities (0.0–7.0 wt.% NaCl equiv.) and CO_2 contents ranging from 14 to 73 mole %. These fluids are very similar to those of some Cretaceous deposits (Yonghwa, Weolseong, Soowang and Weolyu) in the Seolcheon metallogenic province and other Cretaceous gold and silver deposits in Republic of Korea, which are interpreted to be of mainly meteoric origin (Youn and Park, 1991, 1993, 1997, 2004; Yun *et al*., 1993; Lee *et al*., 1994) (Table 4). The fluid compositional range of the Namseong veins is shown on a δD vs. δ^{18}O plot and is compared to the compositional ranges of Yonghwa, Soowang and Weolyu deposits, along with the regions of magmatic waters taken from Taylor (1979) (Fig. 13). The $\delta^{18}O_{water}$ and δD_{water} values from the Namseong deposit correspond to the fluid compositional range $\delta^{18}O_{water}$ –2.2‰ to 1.6‰; δD_{water} –83‰ to –64‰, values that lie between values for magmatic and meteoric water (Fig. 13).

Although most $\delta^{18}O_{water}$ values calculated from these deposits overlap, some calculated $\delta^{18}O_{water}$ values of sericite from Yonghwa and Soowang deposits are higher than those of quartz from the Namseong and Weolyu deposits, which may be consistent with a magmatic signature (Table 4 and Fig. 13), however, oxygen isotope data for the Namseong and Weolyu deposits are compatible with a fluid of meteoric origin. This trend of $\delta^{18}O_{water}$ and δD_{water} values of quartz from the Namseong deposit is similar to that of quartz and calcite reported by Yun *et al*. (1993) and Youn and Park (1997) for the Yongwha, Soowang and Weolyu deposits, indicating input of less evolved meteoric water through the mineralization sequence.

The unmixing of fluids as recorded by inclusions from early white quartz of the Namseong gold-silver deposit is a common phenomenon. Unmixing of a carbonic phase (CO_2, CH_4) from the hydrothermal fluids would lower the δ^{18}O and δD values of the remaining aqueous component because of the large fractionation between carbonic

phases (CO_2, CH_4) and water for oxygen and hydrogen, assuming a Rayleigh process (Horibe and Craig, 1995; Macey and Harris, 2006). However, these phenomena are not apparent in the trend of $\delta^{18}O_{water}$ and δD_{water} values from the Namseong deposit (Fig. 13). Consequently, the hydrothermal fluid that deposited the Namseong veins is interpreted as meteoric in origin, and throughout the mineralization sequence it mixed with less evolved meteoric water.

Conclusions

The three Cretaceous gold and silver-bearing quartz veins from the Namseong deposit occur in Triassic porphyritic granite and include only one stage of quartz veins. The quartz veins contain pyrite, sphalerite, chalcopyrite, galena, electrum, pyrargyrite, argentite and native silver. Two types of fluid inclusions are present in the quartz from the Namseong deposit. Type I inclusions are CO_2–H_2O inclusions and occur only in early stage white quartz. Type II inclusions are aqueous and occur in the early and late stage white and transparent quartz veins. Type I inclusions have minor CH_4 contents, low salinities and moderate homogenization temperatures that are taken to represent minimum trapping temperatures. Type II inclusions have low to moderate salinities and moderate homogenization temperatures. Microthermometric results indicate that the gold and silver-bearing quartz veins are related to H_2O–NaCl–CO_2 and H_2O–NaCl fluids. The H_2O–NaCl–CO_2 fluid produced early wall-rock alteration and sulfide deposition. The H_2O–NaCl fluid was mainly responsible for the gold and silver mineralization.

Gold from the Namseong deposit occurs as electrum associated with mainly late stage sulfides. Gold hydrosulfide was the dominant complex responsible for gold transport during gold mineralization at the Namseong deposit. Gold deposition was mainly caused by a decrease in sulfur fugacity/aH_2S/aCl, oxygen fugacity and temperature accompanying mixing with meteoric water.

Stable isotope results from the Namseong deposit samples indicate that ore sulfur was derived mainly from a magmatic source, but also partly from sulfur in the host rocks. The ore-forming fluids were deeply circulating meteoric water and evolved by mixing with shallower local meteoric water and by limited water-rock exchange during mineralization in uplift zones.

Acknowledgments—The authors would like to thank three Geochemical Journal reviewers for their incisive and helpful reviews that significantly improved the quality and style of this paper. Special thanks are also due to Shogo Tachibana for his dedicated editorial work. We would like to thank S. M. Koh for creative comments. This research was supported by grants from the KIGAM (GP2012-021 and GP2013-021 (13-1121)). EPMA analyses were performed at the Center for Research Facilities of Chungnam National University and stable isotope analyses were performed at the Korea Basic Science Institute and the China University of Geosciences.

References

Baatartsogt, B., Wagner, T., Taubald, H., Mierdel, K. and Markl, G. (2007) Hydrogen isotope determination of fluid inclusion water from hydrothermal fluorite: Constraining the effect of the extraction technique. *Chem. Geol.* **244**, 474–482.

Bakker, R. J. (1997) Clathrates: computer programs to calculate fluid inclusion *V-X* properties using clathrate melting temperatures. *Computers & Geosciences* **23**, 1–18.

Bakker, R. J. (1999) Adaptation of the Bowers and Helgeson (1983) equation of state to the H_2O–CO_2–CH_4–N_2–NaCl system. *Chem. Geol.* **154**, 225–236.

Bakker, R. J. (2003) Package FLUIDS 1. Computer programs for analysis of fluid inclusion data and for modelling bulk fluid properties. *Chem. Geol.* **194**, 3–23.

Barton, P. B., Jr. and Skinner, B. J. (1979) Sulfide mineral stabilities. *Geochemistry of Hydrothermal Ore Deposits* (Barnes, H. L., ed.), 278–403, John Wiley & Sons, New York.

Barton, P. B., Jr. and Toulmin, P., III (1964) The electrum-tarnish method for the determination of the fugacity of sulfur in laboratory sulphide systems. *Geochim. Cosmochim. Acta* **28**, 619–640.

Benning, L. G. and Seward, T. M. (1996) Hydrosulphide complexing of Au (I) in hydrothermal solutions from 150–400°C and 500–1500 bars. *Geochim. Cosmochim. Acta* **60**, 1849–1871.

Bodnar, R. J. (2003) Introduction to fluid inclusions. *Fluid Inclusions: Analysis and Interpretation* (Samsan, I., Anderson, A. and Marshall, O., eds.), *Short Course of the Mineralogical Association of Canada* **32**, 1–8.

Bodnar, R. J. and Vityk, M. O. (1994) Interpretation of microthermometric data for H_2O–NaCl fluid inclusions. *Fluid Inclusions in Minerals: Methods and Applications* (De Vivo, B. and Frezzotti, M. L., eds.), 117–130, VPI Press, Blacksburg, Virginia.

Bowers, T. S. and Helgeson, H. C. (1983) Calculation of the thermodynamic and geochemical consequences of nonideal mixing in the system H_2O–CO_2–NaCl on phase relations in geologic systems: Equation of state for H_2O–CO_2–NaCl fluids at high pressures and temperatures. *Geochim. Cosmochim. Acta* **47**, 1247–1275.

Brown, P. E. (1998) Fluid inclusion modelling for hydrothermal systems. *Techniques in Hydrothermal Ore Deposits Geology* (Richards, J. P. and Larson, P. B., eds.), *Rev. Econ. Geol.* **10**, 151–171.

Brown, P. E. and Hagemann, S. G. (1995) MacFlinCor and its application to fluids in Archaean lode-gold deposits. *Geochim. Cosmochim. Acta* **59**, 3943–3952.

Burruss, R. C. (1981) Analysis of phase equilibria in C–O–H–S fluid inclusions. *Mineralogical Association of Canada Short Course Handbook* **6**, 39–74.

Chappell, B. W. (1999) Aluminium saturation in I- and S-type granites and the characterization of fractionated

haplogranites. *Lithos* **46**, 535–551.
Cheong, C. S. and Chang, H. W. (1997) Sr, Nd, and Pb isotope systematic of granitic rocks in the central Ogcheon belt, Korea. *Geochem. J.* **31**, 17–36.
Cho, W. S., Jwa, Y. J., Lee, J. I. and Lee, M. S. (1994) Petrography and mineral chemistry of the granitic rocks in the Poeun–Sogrisan area, Korea. *J. Petrol. Soc. Korea* **3**, 220–233 (in Korean).
Choi, S. G., Chi, S. J. and Park, S. W. (1988) Gold-silver mineralization of the Au–Ag deposits at Yeongdong district, Chungcheongbuk-do. *J. Korean Mining Geol.* **21**, 367–380 (in Korean).
Choi, S. G., Pak, S. J., Choi, S. H. and Shin, H. J. (2001) Mesozoic granitoid and associated gold-silver mineralization in Korea. *Econ. Environ. Geol.* **34**, 25–38 (in Korean).
Choi, S. G., Kwon, S. T., Ree, J. H., So, C. S. and Pak, S. J. (2005) Origin of Mesozoic gold mineralization in South Korea. *Isl. Arc* **14**, 102–114.
Choi, S. G., Pak, S. J., Kim, S. W., Kim, C. S. and Oh, C. W. (2006) Mesozoic gold-silver mineralization in South Korea: Metallogenic provinces reestimated to the geodynamic setting. *Econ. Environ. Geol.* **39**, 567–581 (in Korean).
Chough, S. K., Kwon, S. T., Ree, J. H. and Choi, D. K. (2000) Tectonic and sedimentary evolution of the Korean peninsula: a review and new view. *Earth-Sci. Rev.* **52**, 175–235.
Clayton, R. N. and Mayeda, T. K. (1963) The use of bromine pentafluoride in the extraction of oxygen from oxide and silicates for isotopic analysis. *Geochim. Cosmochim. Acta* **27**, 43–52.
Cole, D. R. and Drummond, S. E. (1986) The effect of transport and boiling on Ag/Au ratios in hydrothermal solutions: A preliminary assessment and possible implications for the formation of epithermal precious-metal ore deposits. *J. Geochem. Explor.* **25**, 45–79.
Coleman, M. L., Sheppard, T. J., Durham, J. J., Rouse, J. E. and Moore, G. R. (1982) Reduction of water with zinc for hydrogen isotope analysis. *Anal. Chem.* **54**, 993–995.
Collins, P. L. F. (1979) Gas hydrates in CO_2-bearing fluid inclusions and the use of freezing data for estimation of salinity. *Econ. Geol.* **74**, 1432–1444.
Coulibaly, Y., Boiron, M. C., Cathelineau, M. and Kouamelan, A. N. (2008) Fluid immiscibility and gold deposition in the Birimian quartz veins of the Angovia deposit (Yaoure, Ivory Coast). *J. African Earth Sci.* **50**, 234–254.
Dallai, L., Lucchini, R. and Sharp, Z. D. (2004) Techniques for stable isotope analysis of fluid and gaseous inclusions. *Handbook of Stable Isotope Analytical Techniques I* (De Groot, P. A., ed.), 62–87, Elsevier.
Davis, D. W., Lowenstein, T. K. and Spencer, R. J. (1990) Melting behavior of fluid inclusions in laboratory-grown halite crystals in the systems NaCl–H_2O, NaCl–KCl–H_2O, NaCl–$MgCl_2$–H_2O, and NaCl–$CaCl_2$–H_2O. *Geochim. Cosmochim. Acta* **54**, 591–601.
Diamond, L. W. (1992) Stability of CO_2 clathrate hydrate + CO_2 liquid + CO_2 vapour + aqueous KCl–NaCl solutions: Experimental determination and application to salinity estimates of fluid inclusions. *Geochim. Cosmochim. Acta* **56**, 273–280.
Diamond, L. W. (1994) Salinity of multivolatile fluid inclusions from clathrate stability. *Geochim. Cosmochim. Acta* **58**, 19–41.
Diamond, L. W. (2001) Review of systematic of CO_2–H_2O fluid inclusions. *Lithos* **55**, 69–99.
Duan, Z., Møller, N. and Weare, J. H. (1996) A general equation of state for supercritical fluid mixtures and molecular dynamics simulation of mixture PVTX properties. *Geochim. Cosmochim. Acta* **60**, 1209–1216.
Dublyansky, Y. V. and Spötl, C. (2009) Hydrogen and oxygen isotopes of water from inclusions in minerals: design of a new crushing system and on-line continuous-flow isotope ratio mass spectrometric analysis. *Rapid Commun. Mass Sp.* **23**, 2605–2613.
Faure, K. (2003) δD values of fluid inclusion water in quartz and calcite ejecta from active geothermal systems: Do values reflect those of original hydrothermal water? *Econ. Geol.* **98**, 657–660.
Faure, K., Matsuhisa, Y., Metsugi, H., Mizota, C. and Hayashi, S. (2002) The Hishikari Au–Ag epithermal deposit, Japan: Oxygen and hydrogen isotope evidence in determining the source of paleohydrothermal fluids. *Econ. Geol.* **97**, 481–498.
Gibert, F., Pascal, M. L. and Pichavant, M. (1998) Gold solubility and speciation in hydrothermal solutions: Experimental study of the stability of hydrosulphide complex of gold (AuHS°) at 350 to 450°C and 500 bars. *Geochim. Cosmochim. Acta* **62**, 2931–2947.
Goldstein, R. H. (2001) Fluid inclusions in sedimentary and diagenetic systems. *Lithos* **55**, 159–193.
Goldstein, R. H. and Reynolds, T. J. (1994) Systematics of fluid inclusions in diagenetic minerals. *SEPM short course* **31**, 199.
Hagemann, S. G. and Lüders, V. (2003) P–T–X conditions of hydrothermal fluids and precipitation mechanism of stibnite-gold mineralization at the Wiluna lode-gold deposits, Western Australia: Conventional and infrared microthermometric constraints. *Miner. Depos.* **38**, 936–952.
Hagemann, S. G., Brown, P. E. A. and Walde, D. H. G. (1992) Thin-skinned thrust mineralization in the Brasilia fold belt: The example of the old Luziania gold deposit. *Miner. Depos.* **27**, 293–303.
Harris, A. C., Golding, S. D. and White, N. C. (2005) Bajo de la Alumbrera copper-gold deposit: Stable isotope evidence for a porphyry-related hydrothermal system dominated by magmatic aqueous fluid. *Econ. Geol.* **100**, 863–886.
Hayashi, K. and Ohmoto, H. (1991) Solubility of gold in NaCl- and H_2S-bearing aqueous solutions at 250–350°C. *Geochim. Cosmochim. Acta* **55**, 2111–2126.
Haynes, F. M. (1985) Determination of fluid inclusion compositions by sequential freezing. *Econ. Geol.* **80**, 1436–1439.
Hendel, E. M. and Hollister, L. S. (1981) An empirical solvus for CO_2–H_2O–2.6 wt. % salt. *Geochim. Cosmochim. Acta* **45**, 225–228.
Holloway, J. R. (1981) Compositions and volumes of supercritical fluids in the earth's crust. *Fluid Inclusion. Applications to Petrology* (Hollister, L. S. and Crawford, M. L., eds.), *Mineralogical Association Canada Short Course Handbook* **6**, 13–38.
Horibe, Y. and Craig, H. (1995) D/H fractionation in the sys-

tem methane–hydrogen–water. *Geochim. Cosmochim. Acta* **59**, 5209–5217.

Itaya, T., Nagao, K., Inoue, K., Honjou, Y., Okada, T. and Ogata, A. (1991) Argon isotope analysis by a newly developed mass spectrometric system for K–Ar dating. *Mineralogical Journal* **5**, 203–221.

Jwa, Y. J. (1996) Chemical composition of Korean Cretaceous granites in the Gyeongsang basin: I. Major element variation trends. *J. Korean Earth Sci. Soc.* **17**, 318–325 (in Korean).

Jwa, Y. J. (2004) Possible source rocks of Mesozoic granites in South Korea: Implications for crustal evolution in NE Asia. *T. Roy. Soc. Edin-Earth* **95**, 181–198.

Jwa, Y. J., Lee, J. I. and Kagami, H. (1995) New ages of the granitic rocks in the middle Ogcheon belt, Korea. *50th Annual Meeting Geological Society of Korea* **17** (in Korean).

Kim, O. J. (1970) Gold-silver metallogenic provinces in South Korea. *J. Korean Mining Geol.* **3**, 163–167 (in Korean).

Korea Mining Promotion Corporation (1973) *Ore Deposits of South Korea* **5**, 116 (in Korean).

Korea Mining Promotion Corporation (1983) *Drilling Survey Report of Ore Deposits* **6**, 62–63 (in Korean).

Korea Mining Promotion Corporation (1987) *Ore Deposits of South Korea* **10**, 331 (in Korean).

Kwon, S. H., Park, Y. D., Park, C. S. and Kim, H. S. (2009) Mass-balance analysis of bulk-rock chemical changes during mylonitization of a megacryst-bearing granitoid, Cheongsan shear zone, Korea. *J. Asian Earth Sci.* **35**, 489–501.

Kwon, S. T. and Lee, D. H. (1992) Petrology and geochemistry of the Ogcheon metabasites in Poun, Korea. *J. Petrol. Soc. Korea* **1**, 104–123 (in Korean).

Lee, H. K., Kim, S. J. and Choi, S. G. (1987) Occurrence of electrum from the Namseong gold mine. *J. Korean Mining Geol.* **20**, 223–234 (in Korean).

Lee, H. K., Yoo, B. C., Jeong, K. Y. and Kim, K. H. (1994) Au–Ag minerals and geneses of Weolyu gold-silver deposits, Chungcheongbukdo, Republic of Korea. *Econ. Environ. Geol.* **27**, 537–548 (in Korean).

Lee, S. G., Shin, S. C., Kim, K. H., Lee, T. J., Koh, H. J. and Song, Y. S. (2010) Petrogenesis of three Cretaceous granites in the Okcheon metamorphic belt, South Korea: Geochemical and Nd–Sr–Pb isotopic constraints. *Gondwana Res.* **17**, 87–101.

Lee, S. M., Kim, S. W. and Jin, M. S. (1987) Igneous activities of the Cretaceous to the early Tertiary and their tectonic implications in South Korea. *J. Geol. Soc. Korea* **23**, 331–337 (in Korean).

Macey, P. and Harris, C. (2006) Stable isotope and fluid inclusion evidence for the origin of the Brandberg West area Sn–W vein deposits, NW Namibia. *Miner. Depos.* **41**, 671–690.

Matsuhisa, Y., Goldsmith, R. and Clayton, R. N. (1979) Oxygen isotope fractionation in the system quartz–albite–anorthite–water. *Geochim. Cosmochim. Acta* **43**, 1131–1140.

Nagao, K. and Itaya, T. (1988) K–Ar age determination method. *Memoirs Geol. Soc. Japan* **29**, 5–21 (in Japanese).

Nagao, K., Nishido, H., Itaya, T. and Ogata, K. (1984) K–Ar age determination method. *Bull Hiruzen Res. Inst.* **9**, 19–38 (in Japanese).

Oh, C. W. (2006) A new concept on tectonic correlation between Korea, China and Japan: Histories from the late Proterozoic to Cretaceous. *Gondwana Res.* **9**, 47–61.

Ohmoto, H. and Rye, R. O. (1979) Isotopes of sulfur and carbon. *Geochemistry of Hydrothermal Ore Deposits* (Barnes, H. L., ed.), 509–567, John Wiley & Sons, New York.

Ramboz, C., Pichavant, M. and Weisbrod, A. (1982) Fluid immiscibility in natural processes: Use and misuse of fluid inclusion data. II. Interpretation of fluid inclusion data in terms of immiscibility. *Chem. Geol.* **37**, 29–48.

Ree, J. H., Kwon, S. H., Pak, Y. D., Kwon, S. T. and Park, S. H. (2001) Pretectonic and posttectonic emplacements of the granitoids in the south central Okchon belt, South Korea: Implications for the timing of strike-slip shearing and thrusting. *Tectonics* **20**, 850–867.

Renders, P. J. and Seward, T. M. (1989) The stability of hydrosulphido- and sulphido-complexes of Au(I) and Ag(I) at 25°C. *Geochim. Cosmochim. Acta* **53**, 245–253.

Ridley, J. and Hagemann, S. G. (1999) Interpretation of post-entrapment fluid-inclusion re-equilibration at the Three Mile Hill, Marvel Loch and Griffins Find high-temperature lode-gold deposits, Yilgarn Craton, Western Australia. *Chem. Geol.* **154**, 257–278.

Rios, F. J., Villas, R. N. and Fuzikawa, K. (2003) Fluid evolution in the Pedra Preta wolframite ore deposit, Paleoproterozoic Musa granite, eastern Amazon craton, Brazil. *South Am. Earth Sci.* **15**, 787–802.

Roedder, E. (1984) Fluid inclusions. *Rev. Miner.* **12**, 646 pp.

Sagong, H. and Jwa, Y. J. (1997) Mineral chemistry and major element geochemistry of the granitic rocks in the Cheongsan area. *J. Petrol. Soc. Korea* **6**, 185–209 (in Korean).

Sagong, H., Kwon, S. T., Cheong, C. S. and Choi, S. H. (2001) Geochemical and isotopic studies of the Cretaceous igneous rocks in the Yeongdong basin, Korea: Implications for the origin of magmatism in pull-apart basin. *Geosciences J.* **5**, 191–201.

Sagong, H., Kwon, S. T. and Ree, J. H. (2005) Mesozoic episodic magmatism in South Korea and its tectonic implications. *Tectonics* **24**, 1–18.

Seitz, J. C. and Pasteris, J. D. (1990) Theoretical and practical aspects of differential partitioning of gases by clathrate hydrates in fluid inclusions. *Geochim. Cosmochim. Acta* **54**, 631–639.

Seward, T. M. (1973) Thio complexes of gold and the transport of gold in hydrothermal ore solutions. *Geochim. Cosmochim. Acta* **37**, 379–399.

Seward, T. M. (1984) The transport and deposition of gold in hydrothermal systems. *Gold '82: Rotterdam* (Foster, R. P., ed.), 165–181, A. A. Balkema Publication.

Seward, T. M. (1989) The hydrothermal chemistry of gold and its implications for ore formation: Boiling and conductive cooling as examples. *Econ. Geol. Mon.* **6**, 398–404.

Shenberger, D. M. and Barnes, H. L. (1989) Solubility of gold in aqueous sulphide solutions from 150 to 350°C. *Geochim. Cosmochim. Acta* **53**, 269–278.

Shepherd, T. J., Rankin, A. H. and Alderton, D. H. M. (1985) *A Practical Guide to Fluid Inclusion Studies*. Blackie Sons Ltd., Glasgow, 293 pp.

Sheppard, S. M. F. (1986) Characterization and isotope varia-

tions in natural waters. *Rev. Miner*. **16**, 165–183.

Simon, K. (2001) Does δD from fluid inclusion in quartz reflect the original hydrothermal fluid? *Chem. Geol*. **177**, 483–495.

So, C. S. and Yun, S. T. (1997) Jurassic mesothermal gold mineralization of the Samhwanghak mine, Youngdong area, Republic of Korea: Constraints on hydrothermal fluid geochemistry. *Econ. Geol*. **92**, 60–80.

So, C. S., Yun, S. T. and Shelton, K. L. (1995) Mesothermal gold vein mineralization of the Samdong mine, Youngdong mining district, Republic of Korea. *Miner. Depos*. **30**, 384–396.

Stefánsson, A. and Seward, T. M. (2003) Stability of chloridogold(I) complexes in aqueous solutions from 300 to 600°C and from 500 to 1800 bar. *Geochim. Cosmochim. Acta* **67**, 4559–4576.

Stefánsson, A. and Seward, T. M. (2004) Gold(I) complexing in aqueous sulphide solutions to 500°C at 500 bar. *Geochim. Cosmochim. Acta* **68**, 4121–4143.

Tagirov, B. R., Salvi, S., Schott, J. and Baranova, N. (2005) Experimental study of gold-hydrosulphide complexing in aqueous solutions at 350–500°C, 500 and 1000 bars using mineral buffers. *Geochim. Cosmochim. Acta* **69**, 2119–2132.

Taylor, H. P. (1979) Oxygen and hydrogen isotope relationships in hydrothermal mineral deposits. *Geochemistry of Hydrothermal Ore Deposits* (Barnes, H. L., ed.), 236–277, John Wiley & Sons, New York.

Thiéry, R., Van den Kerkhof, A. M. and Dubessy, J. (1994) VX properties of CH_4–CO_2 and CO_2–N_2 fluid inclusions modelling for $T < 31$°C and $P < 400$ bar. *Eur. J. Mineral*. **6**, 753–771.

Van den Kerkhof, A. M. and Hein, U. F. (2001) Fluid inclusion petrography. *Lithos* **55**, 27–47.

Van den Kerkhof, A. M. and Thiéry, R. (1994) Phase transitions and density calculation in the CO_2–CH_4–N_2 system. *Fluid Inclusions in Minerals: Methods and Applications* (Vivo, B. D. and Frezzotti, M. L., eds.), 171–190, Short Course of the International Mineralogical Association, Inclusions in Minerals Working Group "Inclusion in Minerals".

Van den Kerkhof, A. M. and Thiéry, R. (2001) Carbonic inclusions. *Lithos* **55**, 49–68.

Verheyden, S., Genty, D., Cattani, O. and Van Breukelen, M. R. (2008) Water release patterns of heated speleothem calcite and hydrogen isotope composition of fluid inclusions. *Chem. Geol*. **247**, 266–281.

Yao, Y., Murphy, P. J. and Robb, L. J. (2001) Fluid characteristics of granitoid-hosted gold deposits in the Birimian Terrane of Ghana: A fluid inclusion microthermometric and Raman spectroscopic study. *Econ. Geol*. **96**, 1611–1643.

Yin, J. W., Kim, S. J., Lee, H. K. and Itaya, T. (2002) K–Ar ages of plutonism and mineralization at the Shizhuyuan W–Sn–Bi–Mo deposit, Hunan Province, China. *J. Asian Earth Sci*. **20**, 151–155.

Youn, S. T. and Park, H. I. (1991) Gold and silver mineralization in the Yonghwa mine. *J. Korean Mining Geol*. **24**, 107–129 (in Korean).

Youn, S. T. and Park, H. I. (1993) Gold and silver mineralization in the Weolseong mine. *J. Korean Earth Sci. Soc*. **14**, 263–273 (in Korean).

Youn, S. T. and Park, H. I. (1997) Stable isotope study of gold-silver deposits in the Muju–Youngdong area. *J. Korean Earth Sci. Soc*. **18**, 60–69 (in Korean).

Youn, S. T. and Park, H. I. (2004) Gold and silver mineralization of the Soowang ore deposits in Muju, Korea. *J. Korean Earth Sci. Soc*. **25**, 484–494 (in Korean).

Yun, H. S. and Kim, S. E. (1990) Petrology and petrochemistry of the Cretaceous granites in the southern Mungyeong area. *J. Korean Mining Geol*. **23**, 343–353 (in Korean).

Yun, S. T., So, C. S., Choi, S. H., Shelton, K. L. and Koo, J. H. (1993) Genetic environment of germanium-bearing gold-silver vein ores from the Wolyu mine, Republic of Korea. *Miner. Depos*. **28**, 107–121.